Investigation of New Particle Formation mechanisms and aerosol processes at the Marambio Station, Antarctic Peninsula.

Lauriane Lucie Josette Quéléver [1], Lubna Dada [1,2,3], Eija Asmi [4,5], Janne Lampilahti [1], Tommy Chan [1], Jonathan Ferrara [4], Gustavo Copes [4], German Pérez-Fogwill [4], Luis Barreira[5], Minna Aurela[5], Douglas Worsnop [1,6], Tuija Jokinen [1,7], and Mikko Sipilä [1]

[1] Institute for Atmospheric and Earth System Research / INAR-Physics, P.O. Box 64, FI-00014 University of Helsinki, Finland.

[2] Extreme Environments Research Laboratory, École Polytechnique Fédérale de Lausanne (EPFL) Valais, Sion, 1951, Switzerland

[3] Laboratory of Atmospheric Chemistry, Paul Scherrer Institute, 5232 Villigen, Switzerland

[4] Servicio Meteorológico Nacional / SMN, Av. Dorrego, 4019, Buenos Aires, Argentina

[5] Finnish Meteorological Institute / FMI, Erik Palmenin aukio 1, FI-00560 Helsinki, Finland

[6] Aerodyne Research, Inc. Billerica, MA 01821, USA

[7] The Cyprus Institute, The Climate & Atmosphere Research Centre (CARE-C), P.O. Box 27456 Nicosia, Cyprus

Corresponding Author:

Lauriane L. J. Quéléver (lauriane.quelever@helsinki.fi), Mikko Sipilä (mikko.sipila@helsinki.fi)

Abstract

Understanding chemical processes leading to the formation of atmospheric aerosol particles is crucial to improve our capabilities in predicting the future climate. However, those mechanisms are still inadequately characterized, especially in polar regions. In this study, we report observations of neutral and charged aerosol precursor molecules and chemical clusters composition (qualitatively and quantitatively), as well as air ions and aerosol particle number concentrations and size distributions from the Marambio research station (64° 15’ S - 56° 38’ W), located North of the Antarctic Peninsula. We conducted measurements during the austral summer, between 15 January and 25 February 2018. The scope of this study is to characterize new particle formation (NPF) event parameters and connect our observations of gas phase compounds with the formation of secondary aerosols to resolve the nucleation mechanisms at the molecular scale. NPF occurred on 40 % of measurement days. All NPF events were observed during days with high solar radiation, mostly with above freezing temperatures and, with low relative humidity. The averaged formation rate for 3 nm particles (J_3) was 0.686 cm^{-3} s^{-1} and the average particle growth rate ($GR_{3.8\text{-}12\ nm}$) was 4.2 nm h^{-1}. Analysis of neutral aerosol precursor molecules showed measurable concentrations of iodic acid (IA), sulfuric acid (SA) and methane sulfonic acid (MSA) throughout the entire measurement period with significant increase of MSA and SA concentrations during NPF events. We highlight SA as a key contributor to NPF processes, while IA and MSA would likely only contribute to particle growth. Mechanistically, anion clusters containing ammonia/ dimethylamine (DMA) and SA were identified, suggesting significant concentration ammonia and DMA as well. Those species are likely contributing to NPF events since SA alone is not sufficient to explain observed nucleation rates. Here, we provide evidence of the marine origin of the measured chemical precursors and discuss their potential contribution to the aerosol phase.

1 Introduction

Atmospheric aerosol particles impact the planetary energy budget and radiation balance by influencing cloud optical properties and cloud lifetime (IPCC, 2013). Even though they are crucial for regulating the climate, aerosol particles remain insufficiently characterized, especially in remote regions (Schmale et al., 2019). Understanding the atmospheric processes in places where anthropogenic influence is minimal, such as polar regions, is important for characterizing the pre-industrial-like atmosphere. At the same time, polar environments are significantly impacted by human-induced climate change and are warming twice as fast as the global average (Stuecker et al., 2018). Additionally, polar ecosystems and landscapes are more and more being disturbed by increasing average temperatures that further affect emissions of trace gases into the atmosphere.

Aerosol particles have been observed and characterized in many places in the Arctic and Antarctica (Shaw, 1979; Shaw, 1988; Asmi et al., 2010; Kerminen et al., 2018; Sipilä et al., 2016; Dall´Osto et al., 2017; Jokinen et al., 2018; Dall´Osto et al., 2018; Herenz et al., 2019; Baccarini et al., 2020; Dall'Osto et al., 2019; Beck et al., 2021; Brean et al., 2021). Antarctic primary particles, mainly originating from sea spray or blowing snow, only weakly contribute to total particle number concentration (Lachlan-Cope et al., 2020). Modelling studies have estimated that primary particles would only contribute to ~2 % of the total particle count that the ground level in Antarctica (Merikanto et al., 2009). Secondary formation of aerosol particles, on the other hand, is believed to be the principal contributor to cloud condensation nuclei (CCN), especially in the Antarctic peninsula were models showed contributions varying from 75 % up to 100 % (Jokinen et al., 2018; Kerminen et al., 2018; Merikanto et al., 2009). These secondary aerosols originate from nucleation of gas phase molecules, typically condensing oxidation products of locally or regionally emitted vapors. Once formed, neutral or charged molecular clusters can grow by condensation of gases to sizes where they can act as CCN. The process of aerosol nucleation followed by subsequent growth is called new particle formation (NPF). Only a few studies have observed nucleation mode particles (sub-10 nm) from Antarctica - including oceanic, coastal, and continental areas (Asmi et al., 2010; Virkkula et al., 2009; Järvinen et al., 2013; Kyrö et al., 2013; Weller et al., 2015; Jokinen et al., 2018; Kerminen et al., 2018; Lachlan-Cope et al., 2020; Brean et al., 2021) - and only two of those report molecular clusters forming from precursor gases in coastal sites (Jokinen et al., 2018; Brean et al., 2021).

Previously identified aerosol precursor vapors include sulfuric acid (H_2SO_4, SA, e.g., Kulmala et al., 2013; Sipilä et al., 2010), iodic acid (HIO_3, IA, Sipilä et al., 2016; Baccarini et al., 2020) and iodous acid (HIO_2, He et al., 2021), or highly oxygenated organic molecules (HOM, e.g., Ehn et al., 2014; Bianchi et al., 2019; Kirkby et al., 2016). On the other hand, nucleating ion clusters such as bisulfate ions with SA and ammonia (e.g., Kirkby et al., 2011; Yan et al., 2018; Jokinen et al., 2018; Beck et al., 2021), bisulfate ions and neutral SA with dimethyl amine ($(CH3)_2NH$, DMA, Kürten et al., 2014), were previously identified to participate in aerosol formation processes.

At Marambio, Aboa, and Princess Elisabeth coastal Antarctic stations, air mass trajectories during NPF events indicated a dominant role of the Southern Ocean as a source of aerosol particles, which chemical aerosol composition analysis confirmed by the abundancy of e.g., marine-originated sulfates (Asmi et al., 2010; Herenz et al., 2019; Jokinen et al., 2018). These studies suggest that NPF is linked to sulfur-containing compounds originating from dimethyl sulfide ($(CH_3)_2S$, DMS). At the Antarctic coast, oceanic DMS concentrations are the highest during December to January (i.e., austral summer) with concentration that could exceed 15 nM within the upper 10 m layer of the ocean around the Peninsula compared to a yearly average of ~ 5 nM (Lana et al., 2011). DMS has two well-known oxidation products formed from gas-phase reaction with OH radicals: SA (formed via sulfur dioxide, SO_2) and methane sulfonic acid (CH_3SO_3H, MSA), which can then initiate particle formation and subsequent particle growth (Barnes et al., 2006; Mardyukov and Schreiner, 2018).

IA was also found to significantly contribute to NPF in marine and polar environments (Sipilä et al., 2016; Baccarini et al., 2020; He et al., 2021). Although the chemical production of IA is not fully resolved, IA results from the oxidation of reactive iodine (in the form of I_2, HIO, or intermediate I, He et al., 2021) sourcing from algae/phytoplankton emissions contained within the sea water/ice/snow and exchanged into the atmosphere (Saiz-Lopez and Von Glasow, 2012). At the Antarctic Peninsula, the Weddell Sea – that undergoes consistent and recurrent phytoplankton bloom episodes every early spring - is a potential reservoir for iodic acid emissions, especially due to slower ice retreat during the austral summer and colder sea surface temperature than the Southern Ocean or than the Bellingshausen Sea, on the north and west-side of the peninsula, respectively (Atkinson et al., 2012; Von Berg et al., 2020).

This work aims at charactering the gas-phase aerosol precursors naturally emitted from the marine/ice ecosystem and from the Antarctic continent with comprehensive gas phase and aerosol measurements performed at the Marambio research station, Antarctica. We present our results characterizing atmospheric NPF events observed in the Antarctic Peninsula (in section 3.2). There, we provide an extensive analysis of number size distributions of atmospheric aerosols and naturally charged ions, from ~1 nm to 800 nm. We also report the formation rates (*J*) and growth rates (*GR*) of the observed particle formation events. Our core analysis (in section 3.3) describes gas-phase composition and NPF precursors by mass spectrometry measurements of the concentration of SA, MSA and IA (cf. section 3.3.1) and by identifying the composition of ambient ions present during NPF events (cf. section 3.3.2). Finally, in chapter 4, we combine our results for the chemical composition of both gas- and aerosol-phases to discuss sources of precursor vapors producing secondary aerosol in the Antarctic Peninsula.

2 Methods

2.1 Measurement site

In-situ atmospheric gas- and particle-phase measurements were performed at the Argentinian Antarctic Station Marambio (64° 15'S - 56° 38' W) located on the Seymour Island in the northeastern-most part of the Antarctic Peninsula. Geographically (cf. Fig. 1), the island is on the north edge of the Weddell Sea. The station is operated year-round, with extensive scientific and logistic activities during the austral summer. The campaign instrumentation was located inside a laboratory container, specifically designed for continuous atmospheric composition measurements, sufficiently away (approx. 800 m) from the station main buildings and ideally placed fore-wind from the airstrip to avoid interfering contamination signals in our measurements. Comprehensive measurements of atmospheric composition and meteorology have been carried out in this location since 2013. A description of the Marambio station surroundings, the measurement container, and some previous results can be found in earlier publications, e.g., Asmi et al. (2018).

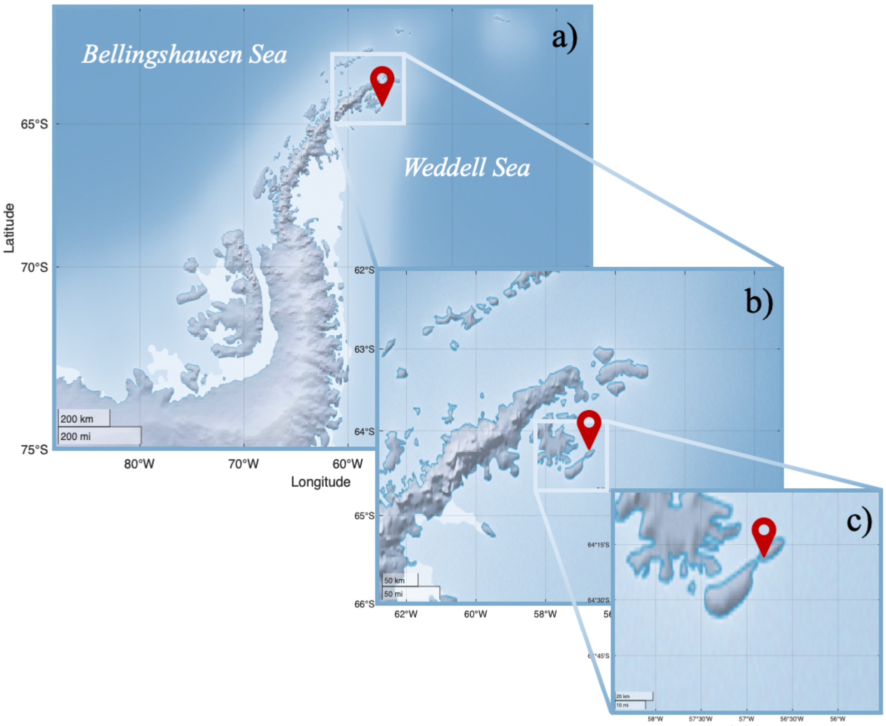

Figure 1: Map of the Antarctic Peninsula, a), with zoom in the north sector, b), and in the Seymour Island with the Marambio station, in c). The measurement location is indicated by the red pin in every panels.

2.2 Austral summer campaign 2018

The austral summer campaign 2018 for measuring the precursors contributing to NPF at the Marambio station was planned for the warm season, when the probability of NPF occurrence is high (Fiebig et al., 2014; Kerminen et al., 2018). The aim was to characterize NPF events, formation, and growth parameters, and resolve the aerosol chemical precursors from their source to their chemical pathways leading to nucleation. We measured concentrations of size segregated aerosol particles (~ 1 – 800 nm diameter) from 19 January to 23 February and chemical information of possible gas-phase precursors from 30 January to 20 February, continuously (whenever possible).

2.3 Instrumentation

Measurements of aerosols and their gas-phase precursors

We deployed a large suite of instruments, briefly described below. Instrument principles and operations are given in detail in the *Supplementary Information*.

(1) The chemical composition and concentration of neutral molecules was measured by a nitrate-based chemical ionization atmospheric pressure interface time of flight (CI-APi-TOF, Tofwerk A.G.) mass spectrometer (Jokinen et al., 2012). Its high-resolution analysis identifies and quantifies potential ambient gas-phase aerosol precursors, such as SA, MSA, IA, or HOM. In some instances, we used the APi-TOF to directly measure atmospheric ions (i.e., naturally charged anions or cations), allowing only atmospheric ions to enter the instruments (i.e., with no added chemical ionization) (cf. *Supplementary information*).

(2) A nano condensation nucleus counter (nCNC) combining a particle size magnifier (PSM, Airmodus Ltd.) with a condensation particle counter (CPC, Airmodus Ltd.) was employed to measure nano-particle concentration in the diameter range from 1 nm to 3 nm. The instrumentation and data inversions are extensively described in Vanhanen et al. (2011), Kangasluoma et al. (2016), Chan et al. (2020) and Lehtipalo et al. (2022) (cf. *Supplementary information*).

(3) A neutral cluster and air ion spectrometer (NAIS, Airel Ltd., Mirme and Mirme, 2013) provided number size distributions of neutral particles and naturally charged atmospheric clusters in the size range from 2 to 42 nm and from 0.8 to 42 nm, respectively. NAIS is well described in the literature and was operated according to the instructions of Manninen et al., 2016. (cf. *Supplementary information*).

(4) Aerosol particle size distributions were measured with a differential mobility particle sizer (DMPS): a Vienna-type differential mobility analyzer for particle size separation (Wiedensohler et al., 2012), followed by a condensation particle counter (CPC; TSI model 3772) for particle counting. The particle size distribution was measured in 25 separate size bins at a 6-minute time resolution. This measurement has been carried out continuously since the year 2013 but only data measured during the summer 2018 campaign are presented here. (cf. *Supplementary information*).

The CI-APi-TOF, nCNC and NAIS were operated with individual (horizontal) inlet lines with a minimum length (1 m, 0.8 m, and 0.9 m, respectively) to minimize losses of nanoparticles. The DMPS was operated in the station's common inlet (PM_{10}, Asmi et al., 2018) and equipped with an additional PM_1 cyclone to prevent super micron particles from entering the setup.

Ancillary measurements

Meteorological parameters were measured on the roof of the measurement container and recorded on a data logger (QML201L, Vaisala Ltd.) since 2013. Measured parameters include temperature and relative humidity (HMP155, Vaisala Ltd.), atmospheric pressure (PTB220, Vaisala Ltd.), wind speed and wind direction (ultrasonic anemometer: Thies 2D, Thies Clima), and radiation (pyranometer: CMP11, Kipp&Zonen).

Chemical composition of the aerosol phase

Aerosol samples for chemical analysis were collected using a virtual impactor (VI, Loo and Cork, 1988), in which particles were divided to two size fractions: fine ($D_p < 2.5$ μm) and coarse (2.5 μm $< D_p <$ 10 μm). Flow rate of the VI was 16.7 L min^{-1}, of which 15 L min^{-1} is used to collect the fine particles and the remaining 1.7 L min^{-1} is used for collection of the coarse particles. Particles were collected on 47-mm Teflon filters. Sampling time was one week. Collected filters were stored on petri slides and kept in a freezer (-18 °C) until analysis.

The mass concentrations of sodium (Na^+), ammonium (NH_4^+), potassium (K^+), magnesium (Mg^{2+}), calcium (Ca^{2+}), chloride (Cl^-), nitrate (NO_3^-), sulphate (SO_4^{2-}), MSA and oxalate ($C_2O_4^{2-}$) were determined from the filter substrates. Cation and anion analyses were done simultaneously with two ion chromatography systems (Dionex, ICS-2000). Filters were extracted in 10 mL of Milli-Q water with 10-min gentle rotation just before chemical analysis. The uncertainty of the IC analysis was estimated according to the analysis of standards as 5 % to 10 %, depending on the ion analyzed. In this study chemical composition of the fine particles is only presented.

2.4 Characteristics of New Particle Formation events

NPF events were identified based on the appearance of particles in the nucleation mode (3 - 25 nm) showing signs of growth (e.g., particles reaching > 10 nm). A classification method was originally proposed by Dal Maso et al. (2005) based on DMPS data. In this study, we combined both DMPS and NAIS data to extend our observations to smaller sizes (Dada et al., 2018).

Condensation sink (*CS*, s^{-1}), which is a measure of how rapid precursor vapor concentrations are lost to pre-existing particles, was calculated using the particle number size distribution measured by the DMPS following the method proposed by Kulmala et al. (2012).

Growth rates (*GR*) of particles between 3.8 nm to 12 nm were calculated using the 50 % appearance time method (Lehtipalo et al., 2014; Dada et al., 2020). Formation rates ($J_{1.5}$, J_3, J_5, and J_{10}) were calculated using the balance equation where the change in concentration of particles inside a size bin is equivalent to the sources (J_{Dp}) minus the available sinks (F_{Coag}+ F_{Growth}), as in Kulmala et al. (2012).

$$(1)\ J_{Dp} = \frac{dN_{Dp}}{dt} + CoagS_{Dp} \cdot N_{Dp} + \frac{GR}{\Delta_{Dp}} \cdot N_{Dp}$$

where *Dp* represents the lower diameter of the bin, N_{Dp} is the particle number concentration inside the size bin, and *GR* is the growth rate of particles out of the bin. Δ_{Dp} is the difference between the upper and lower ends of the size bin of interest.

The coagulation sink ($CoagS_{Dp}$) is a measure of how rapid freshly formed particles of diameter *Dp* are lost to pre-existing particles by collision or coalescence and is calculated as follows:

$$(2)\ CoagS_{Dp} = \int K(Dp, Dp')\, n\, (Dp')\, dDp' \cong \sum_{Dp=Dp}^{Dp\prime=maxK} K(Dp, Dp')\, N_{Dp\prime}$$

where $K\ (Dp,\ Dp')$ is the coagulation coefficient of particle sizes *Dp* and *Dp',* those inside the bin of J_{Dp} and those of pre-existing particles, respectively. $N_{Dp'}$ is the number concentration of the pre-existing particles.

In this work, the formation rates of 1.5 nm particles ($J_{1.5}$) were calculated using nCNC data in the size range of 1.5 nm to 3 nm. Formation rates J_3, J_5 and J_{10} were calculated using NAIS data (total particle mode – using the differencial mobility analyzer of negative voltage) at the size ranges of 3 - 7 nm, 5 - 9 nm, and 10 - 14 nm, respectively. During events when the *GR* could not be calculated (i.e., four events in total) – due to the absence of continuous growth within the size ranges -, a median growth rate calculated of all the events occurring in the same month was used to estimate the formation rate as described by Kulmala et al. (2022).

In addition, the charged particle formation rates ($J^{\pm}_{1.5}$ and $J^{\pm}_{2}$) were calculated using ion number concentration measured by NAIS in both polarities, whenever possible, to determine the contribution of ion induced nucleation to the overall formation rate, according to the following equation:

$$(3)\ J^{\pm}_{Dp} = \frac{dN^{\pm}_{Dp}}{dt} + CoagS_{Dp} \cdot N^{\pm}_{Dp} + \frac{GR}{\Delta Dp} \cdot N^{\pm}_{Dp} + \alpha \cdot N^{\pm}_{Dp} \cdot N^{\pm}_{<Dp} - \chi \cdot N_{Dp} \cdot N^{\pm}_{<Dp}$$

where $N^{\pm}_{Dp}$ is the concentration of ion in a given size range with a lower limit of 1.5 or 2 nm (depending on the J associated size range) and the upper limit ΔDp being larger than that. The coefficient α is the ion-ion recombination coefficient and χ is the ion-aerosol attachment coefficient. α and χ were 1.6×10^{6} cm^{-3} cm^{-1} and 0.01×10^{6} cm^{-3} s^{-1}, respectively (Kulmala et al., 2012).

3 Results

3.1 Ambient conditions: Meteorological parameters

Ambient meteorological conditions during the campaign are presented in Figure 2. Many sunny days are observed, occurring with above-zero degrees Celsius ambient temperatures, high radiation, and relative humidity below 75 %. Even though the measurement site belongs to the Antarctic continent, its position - at relatively high latitude (64° 15’ S) - gives daily solar cycles with zero radiation during the short summer nighttime periods (cf. Fig. 2b). During daytime, higher radiation enhances photo-active emissions from the sea/land ecosystems and promotes atmospheric photochemistry. This is expected to lead to day-time appearance of gas-phase molecules and/or molecular clusters of condensing vapors that can lead to new particle formation and/or aerosol growth. Furthermore, since temperatures above freezing also lead to ice melting (especially in the Weddell Sea area), they are likely to enhance chemical fluxes between thinning ice, ocean, and air (Notz, 2009). These clear sky, warm, sunny days during summertime are known to be optimal weather conditions for NPF to occur in the mid-latitude regions (Dada et al., 2017) and in the Arctic (e.g., Beck et al. 2021) and Antarctic regions (Weller et al., 2015; Jokinen et al., 2018; Baccarini et al., 2020; Brean et al., 2021). Analysis of winds (cf. Fig. 2e) revealed that periods of the highest temperature are seen when wind is blowing from north, bringing warmer air across from the Southern Ocean. Predominant winds were seen from North-Northwest and South-Southwest sectors. The strongest winds were recorded from the South (180°), also driving primarily cold air from the continental plateau, agreeing with Asmi et al. (2018).

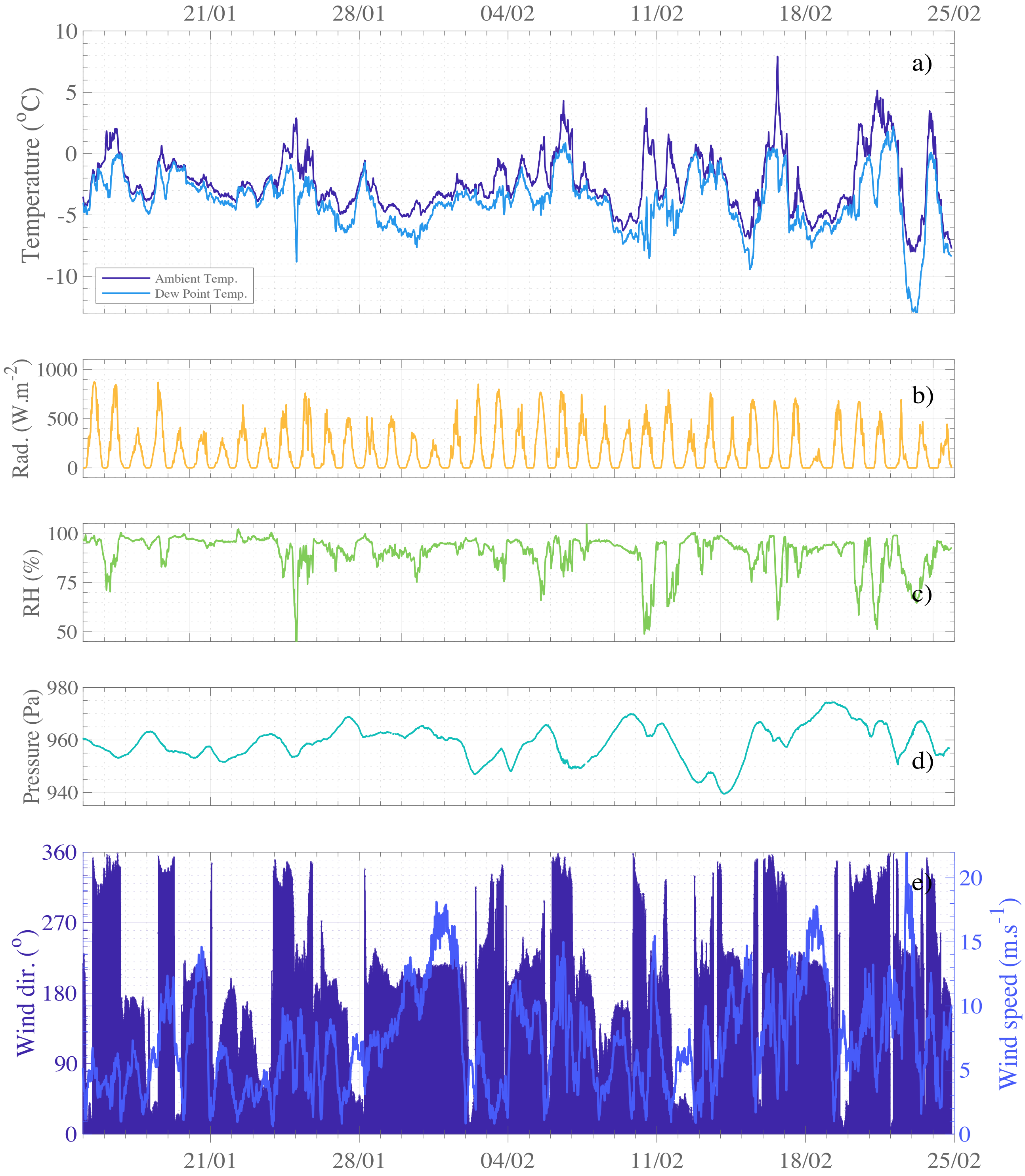

Figure 2: Time series of meteorological parameters: a) temperature (dark blue), dew point (light blue), b) global radiation (orange), c) relative humidity (light green), d) atmospheric pressure (blue green), e) wind direction (dark blue bars) and wind speed (medium blue line). The data are presented with a 10-min resolution and reference time set as local standard, UTC-3.

3.2 Observation & Characterization of NPF events

A total of 13 NPF events (occurring on 12 days) were observed during the 35-day austral summer campaign. Figure 3a shows the continuous size distribution series over the total measurement period from NAIS measurement (size range: 1.8 – 42 nm) and Figure 3b combined the data from nCNC (size shown: 1.2 – 2.7 nm), the NAIS (2.7 nm - 12 nm), and the DMPS (12 nm – 800 nm). Daily number size distribution plots are shown for the 12 event days separately in the *Supplementary Information* (Fig. S3) as well as continuous size distribution series for ion mode (Fig. S4).

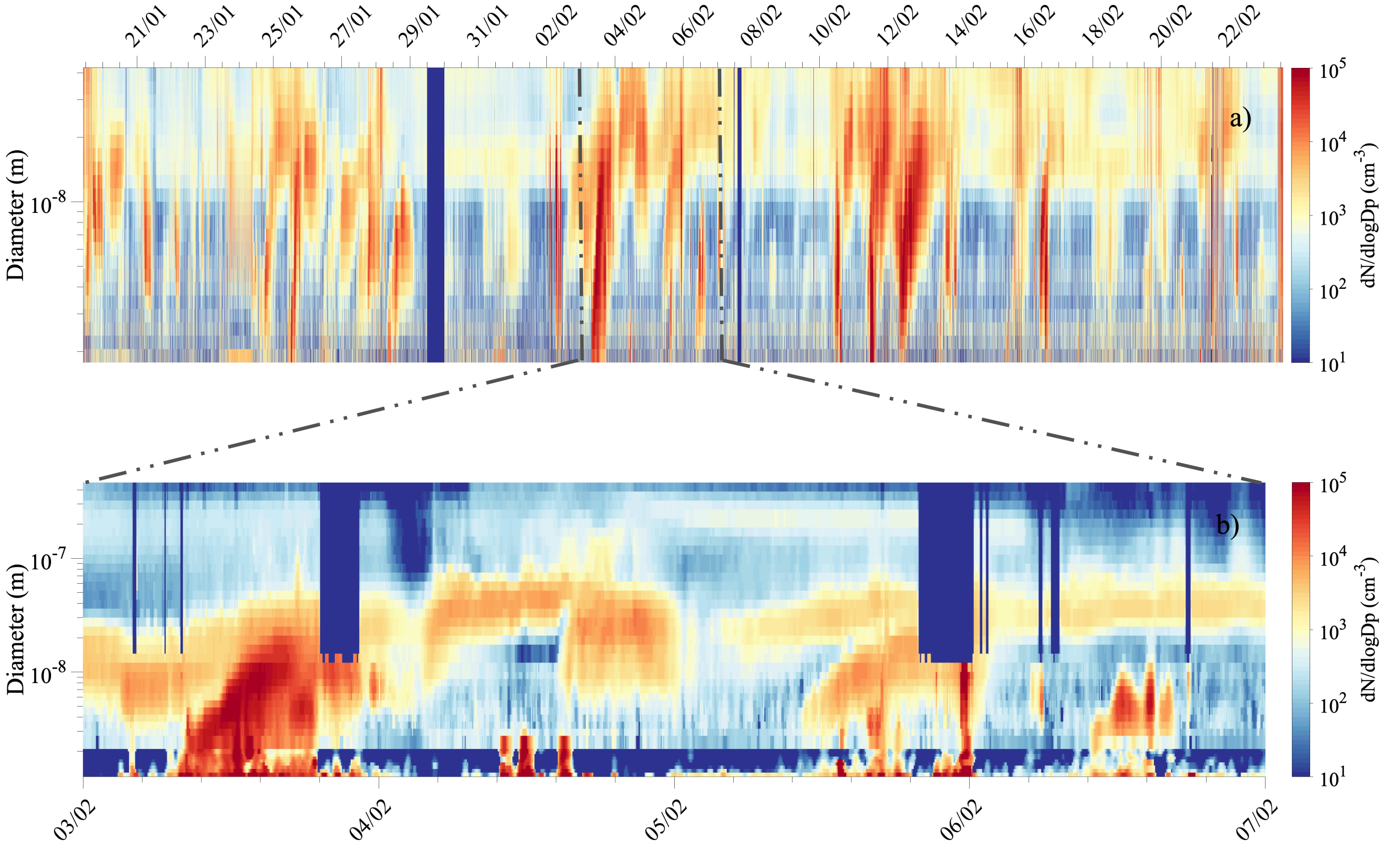

Figure 3: a) Number size distribution from NAIS measurement from 1.8 nm to 42 nm over the whole measurement campaign and **b)** combined size distribution of aerosol particle from 1.2 nm to 800 nm for 3-7 February 2018. The last surface plot combines data from nCNC (1.2 - 2.7 nm), NAIS (particle mode, 2.7 - 12 nm) and DMPS (12-800 nm), whenever the data were available and according to DMPS data flag (only unpolluted data are shown from the DMPS measurements).

On each of the NPF events observed during the campaign, high population of sub-3 nm aerosol particles were seen with concentration larger than 10^4 cm^{-3}. The particles were observed to grow to Aitken mode size range (25 - 100 nm) but rarely reached the accumulation mode sizes (i.e., > 100 nm) (cf. Fig. 3b).

Strong NPF events were identified before midday - local time - (66 % of events), lasting longer than events occurring later in the afternoon. Afternoon events (33 % of the total events) never lasted longer than 2.5 hours. NPF events did vary from day to day: On certain days, growth of the particles was interrupted by abrupt changes in wind direction - resulting in an inability to retrieve a growth or a formation rate within reasonable uncertainty (e.g., 28 January) -; on other days multiple NPF events were observed (e.g., 16 February); or NPF events appeared to have a bumped shape, appearing sporadically - resembling those observed in the Arctic by Beck et al. (2021) – such as the events observed on 28 January and 6 February.

Formation rates were calculated for particle sizes of 1.5, 2, 3, 5 and 10 nm particles, as summarized in Table 1. These formation rates were calculated for the smallest possible particles but also for bigger sizes to ease the comparison with the literature.

Formation rates of 1.5 nm particles (i.e., $J_{1.5}$) were surprisingly high, reaching the maximum rates of 9.2, 10.0, or even 19 cm^{-3} s^{-1}, on February 11th, 10th, and 3rd, respectively. These significantly high values are comparable to those calculated for highly vegetated rural location or even urban areas (e.g., Deng et al., 2020; Kontkanen et al., 2016; Yu et al., 2014), which is surprising due to the remote nature of the environment at our measurement site. For example, formation rates for 1.5 nm particle on the order of 0.030 - 0.013 cm^{-3} s^{-1} were estimated for the Aboa research station - on the other side of the Weddell Sea in East Antarctica (Jokinen et al. 2018). A recent study observing nucleation phenomena at the peninsula close by our measurement location (Brean et al., 2021) found a remarkably high $J_{1.7}$ value reaching up to 3.07 cm^{-3} s^{-1} but still lower than our observed values. Although the formation rates at 1.5 nm are higher than those reported previously, the rates for larger particles (i.e., J_3, J_5, J_{10}) are comparable with the previously reported studies. This discrepancy between formations rates of 1.5 nm particles and of bigger particles could be attributed to favorable nucleation conditions (i.e., sufficient nucleating vapors) but a lack of condensable vapors contributing to particle growth which, in all, reduces the probability of particle survival.

The nucleation rates for 3 nm particles in our study ranged from 0.13 cm^{-3} s^{-1} to 3 cm^{-3} s^{-1} , which were, on average, also significantly higher than 0.03 cm^{-3} s^{-1} $< J_3 <$ 0.14 cm^{-3} s^{-1} reported from Jokinen et al. (2018) study or from Kecorius et al. (2019) who showed J_3 values from 0.080 cm^{-3} s^{-1} to 0.319 cm^{-3} s^{-1} during a polar cruise in the Arctic.

On the other hand, our observation agrees with the J_{10} reported by Kyrö et al. (2013) ranging from 0.003 to 0.3 cm^{-3} s^{-1}, with 0.006 cm^{-3} s^{-1} < J_{10} < 0.37 cm^{-3} s^{-1} in our case.

Additionally, to account for ion induced nucleation, we calculated the formation rates for charged ions of 1.5 nm ($J^{+/-}_{1.5}$) separately using the ion concentrations measured with the (N)AIS in ion mode. The formation rates for positive 1.5 ions, $J^{+}_{1.5}$, ranged from 3.6 × 10^{-4} to 8.3 × 10^{-2} cm^{-3} s^{-1} and $J^{-}_{1.5}$ was from 2.2 × 10^{-3} to 5.4 × 10^{-2} cm^{-3} s^{-1}. Our results are significantly lower than the maximum $J^{-}_{1.5}$ of 0.33 cm^{-3} s^{-1} reported in Beck et al. (2021) or from Kyrö et al. (2013) who showed 0.02 cm^{-3} s^{-1} < $J^{-}_{1.6}$ < 4.2 cm^{-3} s^{-1} - in two coastal Antarctic sites, but in the range reported from the Arctic ocean by Kecorius et al. (2019, e.g., 0.026 cm^{-3} s^{-1} < $J^{-}_{1.6}$ < 0.060 cm^{-3}.s^{-1}). In comparison to 1.5 nm-neutral particle formation rates, the ion formation rates do not represent a major contribution (ratio $J_{neutral}$ /J_{ion} ~ 10^{3}), implying that the relatively high neutral nucleation rates are not primarily due to ion-mediated nucleation.

Particle growth rates were calculated for 3.8 nm to 12 nm diameter size or alternatively up to 11 nm and 8 nm for event #1 and event #13, respectively, whenever the shape of the number size distribution was continuously increasing. Averages for each event are also presented in Table 1. Similarly to formation rates of the smallest particles, the growth rates were remarkably higher (1.2 nm h^{-1} < GR < 10.9 nm h^{-1}) than previously reported for other Antarctic sites. In comparison, Weller et al. (2015) reported growth rates from 3 to 25 nm particles ranging from 0.06 to 0.9 nm h^{-1} at Neumayer III station, Jokinen et al. (2018) showed 0.26 nm h^{-1} < GR < 1.30 nm h^{-1} at Aboa and Brean et al. (2021) published growth rates for 4.5 - 10 nm particles of 0.41 nm h^{-1} to 0.58 nm h^{-1} measured at the Peninsula. Additionally, Kerminen et al. (2018) reviewed aerosol characterization from many different field studies and indicated an upper growth rate estimation of 5.5 nm h^{-1} (as 95th percentile) in Antarctic sites versus 4.1 nm h^{-1} in Arctic environments. Recent Arctic studies by Kecorius et al. (2019) reported 0.62 nm h^{-1} < $GR_{(3\text{-}7\ nm)}$ < 4.25 nm h^{-1} while Collins et al. (2017) reported averaged growth rates of 4.3 ± 4.1 nm h^{-1}.

Table 1: Summary of NPF event classification, formation and growth parameters calculated during the Marambio austral summer campaign. The pollution flag is determined based on DMPS data according to NILU/EBAS format classification at the start time of the event (when data available, 000: clean data, 189: data coming from a possibly polluted sector (e.g., station main buildings), 599: suspected pollution from unknown source). All formation rates are averaged between the start and end of the characterized events.

#	***Date*** *(dd/mm)*	***Start Time*** *(SLT*, hh.mm)*	***Duration*** *(hh.mm)*	***Flag*** *(DMPS)*	***Formation Rates*** ***(J_{size}, cm.s^{-1})***					***Condensation Sink*** *(s^{-1})*	***Growth Rates*** *(Gr_{size}, nm.h^{-1})*
					$J_{1.5}$ ($J_{1.5}^{-}/J_{1.5}^{+}$)	**(J_2^{-}/J_2^{+})**	**J_3**	**J_5**	**J_{10}**		**$Gr_{3.8\text{-}12}$**** ± err.
1	19/01	14.35	0.55	189	-	-	-	-	-	-	9.7 ± 3.2 ($Gr_{3.8\text{-}11}$)
2	24/01	18.30	2.26	-	- ($1.3e^{-2}$ / $1.2e^{-2}$)	($1.2e^{-2}$ / $1.9e^{-2}$)	$6.0e^{-1}$	$3.3e^{-2}$	$6.1e^{-3}$	-	2.4 ± 0.7
3	25/01	14.00	2.25	000	- ($1.2e\text{-}^{2}$ / $9.8e^{-3}$)	($4.9e^{-1}$ / $6.9e^{-1}$)	1.2	$4.7e^{-1}$	$3.7e^{-1}$	$7.5e^{-4}$	10.9 ± 2.8
4	27/01	18.50	2.06	189	4.3 ($3.6e^{-4}$ /$3.6e^{-3}$)	($6.5e^{-3}$/$2.0e^{-2}$)	$6.9e^{-1}$	$7.2e^{-1}$	$1.8e^{-1}$	$3.8e^{-4}$	-
5	28/01	9.13	7.25	000	3.6 ($8.5e^{-3}$ /$6.7e^{-3}$)	($1.9e^{-2}$/$3.4e^{-2}$)	$1.6e^{-1}$	$4.8e^{-2}$	$1.2e^{-2}$	$2.2e^{-4}$	-
6	03/02	8.13	7.04	~000	19.0 ($3.4e^{-2}$/ $2.5e^{-2}$)	(2.9/4.0)	3.0	$5.5e^{-1}$	$2.9e^{-1}$	$1.1e^{-3}$	2.4 ± 0.4
7	05/02	8.35	6.36	000	1.5 ($7.2e^{-3}$/$5.2e^{-3}$)	($3.9e^{-3}$/$4.3e^{-3}$)	$1.8e^{-1}$	$1.3e^{-1}$	$6.8e^{-2}$	$1.3e^{-3}$	1.6 ± 0.7
8	06/02	9.35	4.25	000	1.1 ($8.3e^{-2}$/$5.4e^{-2}$)	(2.7/1.7)	$1.3e^{-1}$	$9.0e^{-3}$	$1.2e^{-2}$	$4.8e^{-4}$	2.4 ± 1.2
9	10/02	11.16	3.52	~000	10.0 ($4.2e^{-3}$/$2.2e^{-3}$)	($1.8e^{-1}$/$2.1e^{-1}$)	$8.3e^{-1}$	$3.6e^{-1}$	$3.6e^{-2}$	$3.7e^{-4}$	-
10	11/02	10.27	6.16	000	9.2 (-/-)	(1.3/$8.9e^{-1}$)	$9.2e^{-1}$	$3.5e^{-1}$	$2.1e^{-1}$	$4.0e^{-4}$	-
11	12/02	10.40	5.40	189	- ($8.1e^{-3}$ /$1.9e^{-2}$)	($4.1e^{-1}$/$5.9e^{-1}$)	2.1	2.7	$1.8e^{-1}$	$2.2e^{-3}$	1.2 ± 0.7
12	16/02	11.18	6.03	599	3.7 ($5.9e^{-2}$/$3.2e^{-2}$)	($7.2e^{-2}$/$4.3e^{-2}$)	$5.9e^{-1}$	$4.0e^{-1}$	$1.2e^{-1}$	$2.4e^{-5}$	3.6 ± 0.7
13					-	-	-	-	-	-	2.2 ± 2.9 ($Gr_{3.8\text{-}8}$)

* *Standard local time, UTC -3*

** *Growth rates were calculated ideally from 3.8 nm to 12 nm. If the growth on that range cannot be determined in that range, the specific range is indicated in subscript as $Gr_{x\text{-}x}$.*

3.3 Chemical composition of the gas-phase precursor molecules

3.3.1 Gas-phase contribution to NPF

Measurements utilizing nitrate based chemical ionization mass spectrometry (CI-APi-TOF) detected gas-phase molecules and molecular clusters that have affinity for proton transfer with nitrate reagent ion. These included SA, MSA, and IA - detected as HSO_4^- and $HNO_3HSO_4^-$ (m/z 96.9601 Th and 159.9557 Th), $CH_3SO_3^-$ and $HNO_3CH_3SO_3^-$ (m/z 94.9808 Th and 157.9765 Th), IO_3^- and $HNO_3IO_3^-$ (m/z 174.8898 Th and 237.8854 Th), respectively. Concentrations were calculated from high resolution peak fitting and reported below. The time series of those compounds during the whole campaign, according to the data availability of the CI operation, are shown in Figure 4.

The measured gas-phase concentrations of the species of interest showed maxima of $\sim 2.6 \times 10^7$ molecules cm^{-3}, $\sim 2.3 \times 10^7$ molecules cm^{-3} and $\sim 3.6 \times 10^6$ molecules cm^{-3} for the total SA, MSA, and IA concentrations, respectively. The three gas-phase compounds seemed to evolve with roughly similar behavior, likely due to favorable weather conditions promoting atmospheric chemical reactions and especially by enhancing photochemical oxidation reactions within a stable boundary layer. A significant and simultaneous increase in SA, MSA, IA concentrations was observed during peaking radiation time close to noon-time – coinciding with local zenith time, i.e., solar noon that is slightly later than midday - and prior to many NPF events, though to a smaller extent for IA. This clearly demonstrates the diurnal nature of the emission of those species, and their transport – especially for SA and IA – as shown in Figure 5. Additionally, it is worth mentioning that even though the MSA concentrations were on average higher than those of SA, event days correlated strongly with peaking SA concentration (then becoming higher than MSA concentration) while IA – whose concentration remained unchanged independently of NPF occurrence - was significantly lower than SA or MSA concentrations.

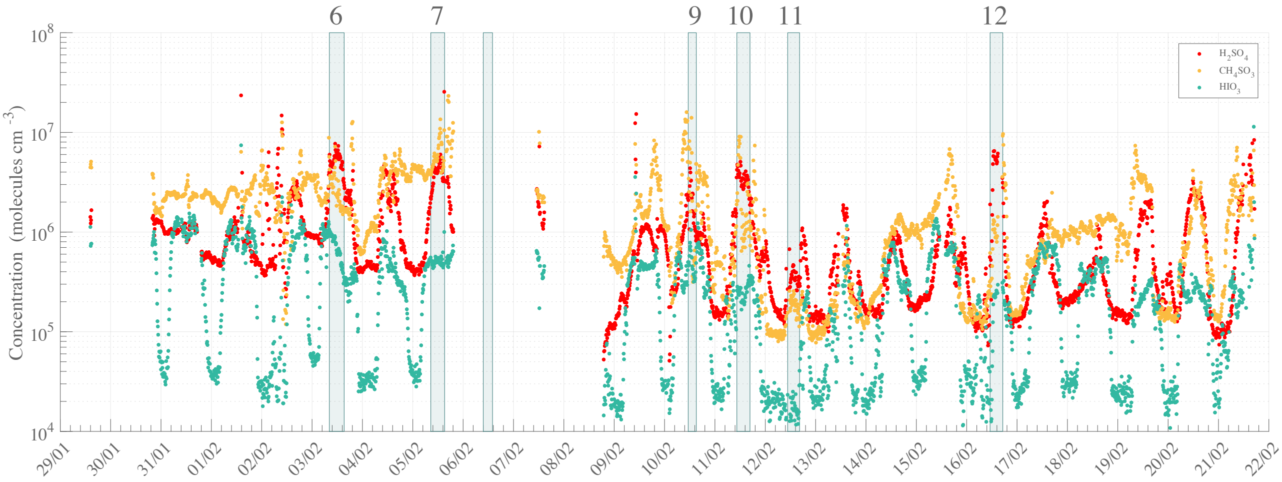

Figure 4: High resolution time series of H_2SO_4 (SA, red), CH_4SO_3 (MSA, orange), HIO_3 (IA, green). Numbers specified on the top of the figure refer to the event number as introduced in the NPF analysis (Cf. Table 1). The data are averaged to 10 min with local time (UTC -3). Note that the missing points are due to switch of the measurement mode and / or data availability.

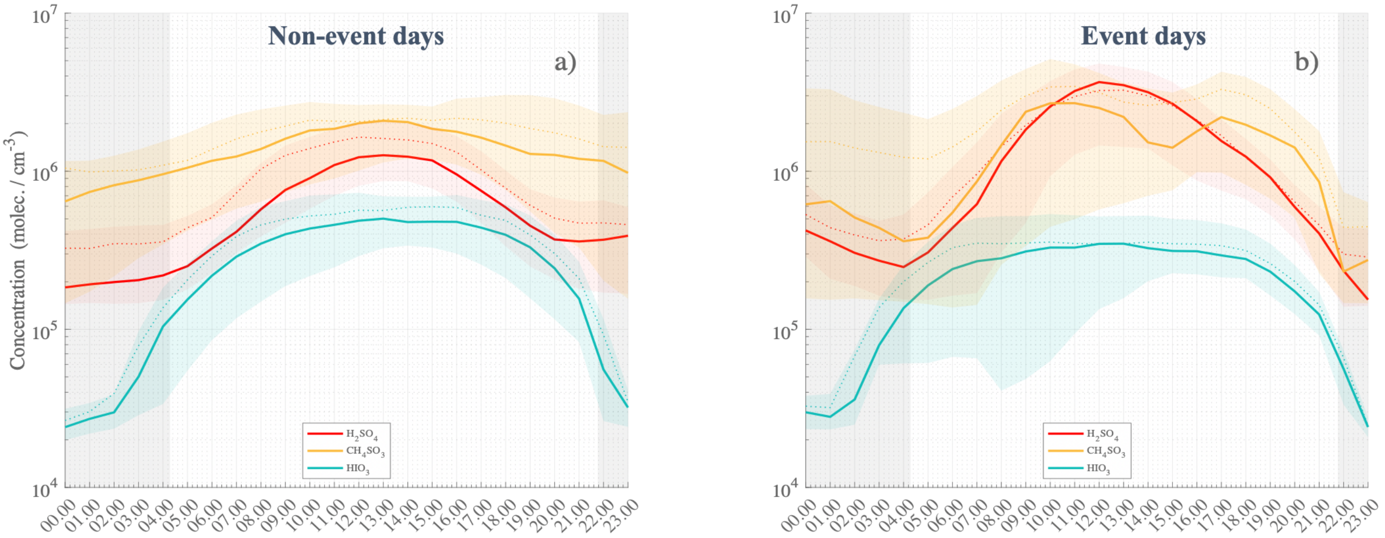

Figure 5: Statistical diurnal time series of H_2SO_4 (SA, red), CH_4SO_3 (MSA, orange), HIO_3 (IA, green) observed during non-event days a) and event days b). The solid lines represent the median hourly average concentrations, the dotted lines are the concentration means and the colored shaded areas show data points within the 25th and the 75th percentiles. Nighttime is represented by the gray-shaded area with median theoretical sunsets and sunrises occurring during the campaign. The actual sunset and sunrise values could vary approx. $^+/_-$ 1.25 hours from the beginning to the end of the campaign.

Figure 5 shows the diurnal variations of SA, MSA and IA for event b) and non-event days a), separately. In both figures, we could see a clear rise in concentrations of SA, MSA and IA throughout the day, with maxima observed at midday.

While both MSA and SA concentrations are on average increasing after sunrise, IA concentration started to increase already during nighttime, shortly after 01:00 SLT, suggesting that strong photochemistry conditions (i.e., direct solar radiation) might not be necessary to produce the observed IA agreeing with He et al. (2021). Earlier studies have shown that IA is even anticorrelated with (still omnipresent) solar radiation in more continental Antarctica (Jokinen et al., 2018). It is likely that even very low levels of solar radiation would be sufficient to saturate the iodic acid production (Beck et al., 2021). Distinctively, a clear difference in the statistical series can be seen between event and non-event days, with more than doubled SA concentrations at zenith-time (factor of 2.25). MSA concentrations are only slightly higher in the morning and afternoon – with an apparent drop occurring from 14:00 to 16:00 – although the starting concentrations at sunrise and sunset are also smaller, depicting strong concentration variability as compared to non-event days. On the other hand, IA is on average lower during event-days – e.g., from ~ 4.5×10^5 molecules cm^{-3} vs ~ 3×10^5 molecules cm^{-3}, with a factor of 1.5 smaller at zenith-time. This last observation indicates that IA is likely not a key contributor to particle formation, while the duo SA-MSA could influence the aerosol phase as already suggested by Beck et al. (2021), Hodshire et al. (2019) and Willis et al. (2016).

3.3.2 Molecular characterization of aerosol / ion precursors: Study case on 16 February

The aerosol event observed on 16 February was particularly interesting due to the occurrence of two consecutive NPF events within the same day. An overview of both aerosol concentrations / parameters and reactive trace gases concentrations for 16 February is shown in Figure 6 with a) the particle number size distribution series from NAIS measurement, b) time series of total particle concentration within several size modes (i.e., cluster, nucleation, Aitken and accumulation), c) estimated J rates for 1.5, 3, 5 and 10 nm particles and d) time series for SA, MSA and IA.

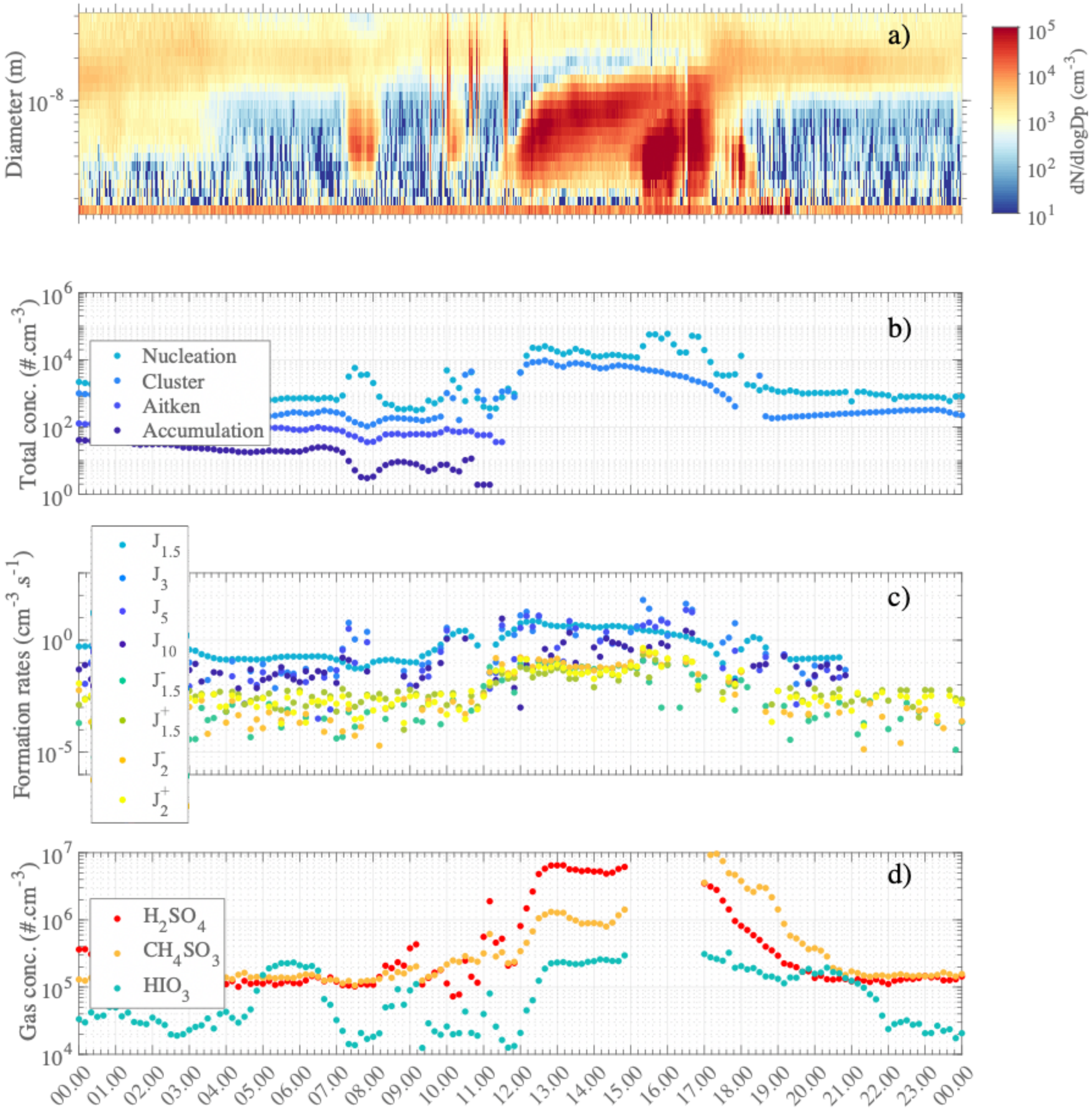

Figure 6: Overview of Aerosol formation event on 16 February 2018: a) Number size distribution from NAIS measurements (Particle mode). b) Concentrations of particles modes (cluster: sub- 3 nm – medium light blue, nucleation: 3 – 25 nm – light blue, Aitken: 25 – 100 nm – medium dark blue, accumulation: 100 – 1000 nm – dark blue). Note that the missing points for Aitken and Accumulation mode are due to data filtering from suspected pollution from the DMPS data set. c) Formation rate estimation for $J_{1.5}$ (neutral - light blue, (-) - blue green, (+) – green), J_2 ((-) - orange, (+) - yellow), J_3 (medium light blue), J_5 (medium dark blue) and J_{10} (dark blue). Note that the formation rate calculation depends on the condensation/coagulation sinks calculated from the DMPS data. d) High resolution time series of H_2SO_4 (red), CH_4SO_3 (orange), HIO_3 (green). Note that the data gap is due to ion mode of APi-measurement. All data are averaged / estimated with a 10 min time resolution, with standard local time (UTC -3) as clock reference.

A clear NPF episode occurred from about 11:15 in the morning until sunset with a net increase of cluster and nucleation mode particle concentrations. Close to noontime all trace gases of interest were significantly increasing (Fig. 6d). MSA increased by almost a factor of 10 by 13:00 ($[\mathrm{MSA}]_{t=13.00}$ = 1.3 × 10^6 molecules cm^{-3}) and by more than 2 orders of magnitude at 16:00 ($[\mathrm{MSA}]_{t=17.30}$ = 9.6 × 10^6 molecules cm^{-3}) as compared by the minimum baseline of ~ 2 × 10^5 molecules cm^{-3} for both MSA and SA. SA maximum concentration was 6.5 × 10^6 molecules cm^{-3}, also observed at 13:00.

IA concentrations were fluctuating throughout the day with maximum concentrations of ~ 2.05 × 10^5 molecules cm^{-3} and ~ 2.35 × 10^5 molecules cm^{-3}, respectively around 05:30 – 06:30 and shortly after 13:00. The net increase of all these gas-phase species occurred quasi-simultaneously as the increase of formation rate of the smallest particles and ions (Fig. 6c), occurring around noon. Interestingly, several sudden, short-lasting increases for all SA, MSA, and IA concentrations were seen even before 13:00, matching bumps in nucleation mode particles around 09:00 and 11:00 and one to two orders of magnitudes increase of cluster mode particles at 11:00. The high concentrations of SA, MSA (and possibly IA) likely trigger the observed aerosol processes (i.e., nucleation and/or growth of particles).

We investigated the mass spectrum further and show a complementary mass spectrum in Figure S2. Any HOM (Bianchi et al., 2019; Ehn et al., 2014) could be reliably resolved from the mass spectra analysis. We estimate that the total oxidized organic contribution, possibly condensable HOM, could not exceed 5.5 × 10^6 molecules cm^{-3}, between 16:30 and 17:30; assuming mass spectral peaks found above 200 Th with positive mass defect could be HOM (*cf. Supplementary*). However, the actual HOM contribution is likely to be only a fraction of this estimation. Therefore, it is unlikely that HOM significantly contributed to nucleation or growth of newly formed particles.

Specifically for this event, we complemented the CI-APi-TOF measurement with negative APi-TOF ambient measurement mode, from 14:52 to 15:53, as reported in Table S1. By showing the divergence of the exact molecular mass of a detected ion in high resolution from its integer mass (i.e., defined as mass defect), a mass defect plot illustrates the mass defect of selected ions (in y-axis) over a studied mass range (in x-axis). Compared to a typical mass spectrum this has the advantage to show the most significant ion population at once, rather independently of signal intensity which is then scaled by the marker size, easing the identification of e.g., clustering mechanisms as further discussed. There, each point of the mass defect plot corresponds to a unique atomic composition. An example of such representation is shown in Figure 6, for the study case of 16 February.

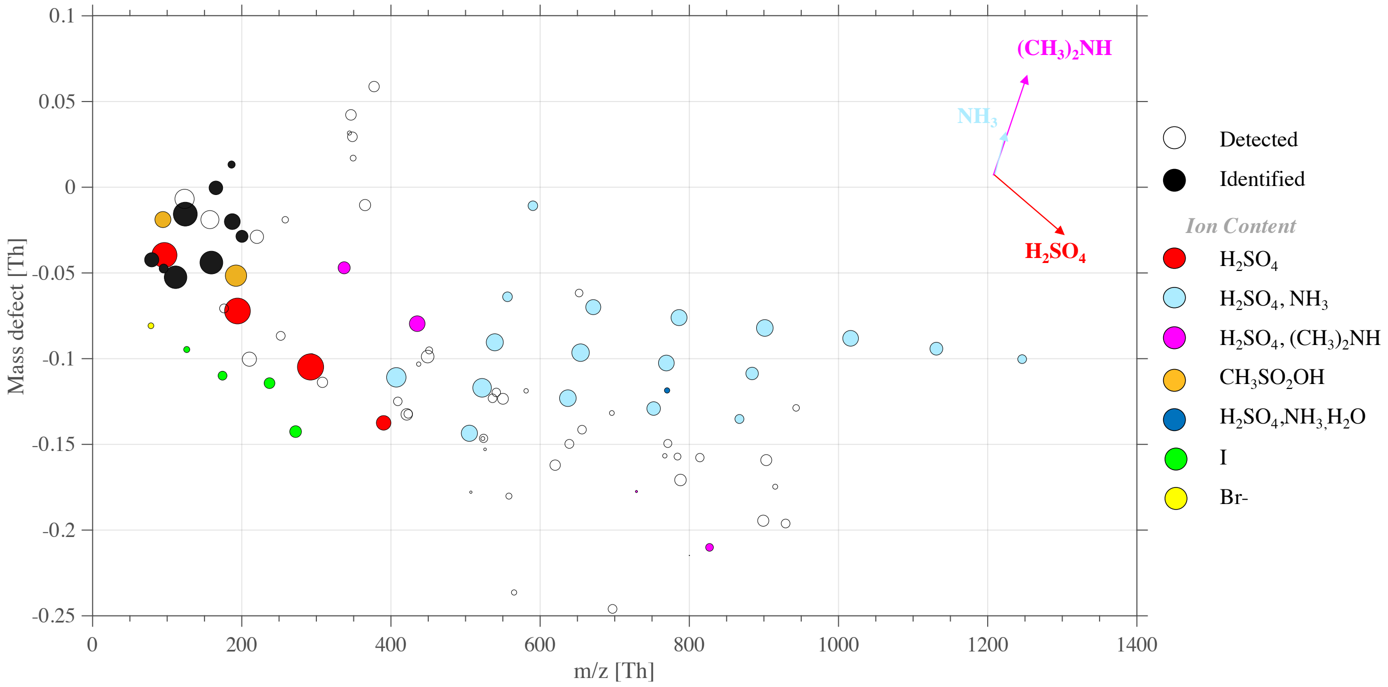

Figure 7: Mass defect plot for (-) APi-TOF measurements, on 16 February from 14:52 to 15:52. The figure type represents the deviation of high resolution fitted peaks exact mass normalized to the unit mass detected for each peak y-axis - e.g. $Br^-_{exact\ mass}$ = 78.9189, $Br^-_{unit\ mass}$ = 79, $Br^-_{mass\ defect}$ = - 0.0811 – while the x-axis represents the mass range (m/z). Data average is 1 hour for each spectrum to improve the signal to noise ratio and the peak shape statistics.

The APi-TOF ion mode showed TIC maximum values around 50 ions s^{-1}, detecting only ions that are naturally charged. The highest signals (i.e., intensity shown by marker sizes, cf. Fig. 7) are bisulfate and its multimers $(H_2SO_4)_{0-4}HSO_4^-$, respectively at m/z = 96.9601, m/z = 194.9275, m/z = 292.8949 and m/z = 390.8622. Along with SA multimers, successive addition of sulfuric acid and ammonia NH_3 formed clusters represented with the light-blue dots, within the mass range 400 – 1250 Th. These sulfuric acid (bisulfate) - ammonia clusters were found with up to 10 additions of H_2SO_4 and 9 NH_3 on top of the HSO_4^- core ion. In line with previous field observations (e.g., Schobesberger et al., 2015; Bianchi et al., 2016; Jokinen et al., 2018; Yan et al., 2018; Beck et al., 2021; Sipilä et al., 2021) and laboratory studies (e.g., Kirkby et al., 2011; Schobesberger et al., 2015) showed that ammonia is detected only in clusters with 3 or more H_2SO_4 molecules around the HSO_4^- core.

The numerous clusters containing both SA and ammonia, as well as the high intensity of the respective cluster signal (depicted by the marker size in Figure 6) suggest a high concentration of such ion group in the gas-phase which also could indicate an ion induced nucleation driven by the ternary system SA-ammonia(-water) - similar to observations made by Jokinen et al. (2018) in East

Antarctica as well as measured in multiple other locations around the globe (e.g., Bianchi et al., 2016; Yan et al., 2018; Beck et al., 2021; Sipilä et al., 2021).

Additional clusters containing SA and DMA (principally as $(H_2SO_4)_2.(CH_3)_2NH.HSO_4^-$ (m/z = 337.9527) and as $(H_2SO_4)_3.(CH_3)_2NH.HSO_4^-$ (m/z = 435.9210) but also one larger cluster, $(H_2SO_4)_7.(CH_3)_2NH.HSO_4^-$ (m/z = 827.7893) was identified. Similarly to the finding of Brean et al. (2021) who detected various SA-amine clusters around the peninsula, SA-DMA-H_2O driven nucleation could also occur leading to formation rates significantly higher than those observed in the SA-NH_3-H_2O system (Kürten et al., 2014; Almeida et al., 2013). In fact, as shown in laboratory studies, (negative) ion composition from APi-TOF analysis likely matches the cluster composition of the neutral clusters in NPF (Schobesberger et al., 2013). The appearance of DMA in the SA dimer and trimer suggests sufficient DMA to trigger nucleation; while the NH_3 in larger clusters is consistent with much higher NH_3 gas concentrations that then dominate nano-particle growth. This highlights that DMA is 1000 times more effective than NH_3 for nucleation; so that sub-ppt DMA and 100 – 1000 ppt levels (and above) of NH_3 could explain the ion cluster distribution observed in Figure 7.

Individual MSA-related ions can be identified (cf. Fig. 7, orange dots) at m/z = 94.9808 and m/z = 192.9482, respectively. Several studies have shown the possible role of MSA in aerosol processes, including nucleation (Hodshire et al., 2019) - especially with involvement on SA-DMA clusters (Bork et al., 2014). However, in our case, MSA was only found as $CH_3SO_3^-$ and as $CH_3SO_3H.HSO_4^-$. MSA was not observed in larger clusters solely composed of SA, NH_3 and DMA and therefore likely does not contribute to the nucleation observed on that day (at least not through to negative ion pathway).

Finally, we identified the presence of halogen compounds, (cf. Fig. 7, yellow and green dots), such as Br^- (m/z = 78.9189), I^- (m/z = 126.9050), IO_3^- (m/z = 174.8898), $HIO_3NO_3^-$ (m/z = 237.8854), $HIO_3HSO_4^-$ (m/z = 272.8571). The presence of halogenated species as natural ions could also indicate that these compounds contribute to aerosol processes. However, these ions were only identified as small halogen clusters of low molecular weight and with only low signal intensity. Considering previous observations in the arctic and coastal environment (Sipilä et al, 2016) only shows iodine-related nucleation as successive addition of multiple iodic acid and water group, it is unlikely that IA promotes nucleation either through neutral or ion-induced mechanism at this Antarctic site.

3.3.3 Chemical composition of the aerosol phase

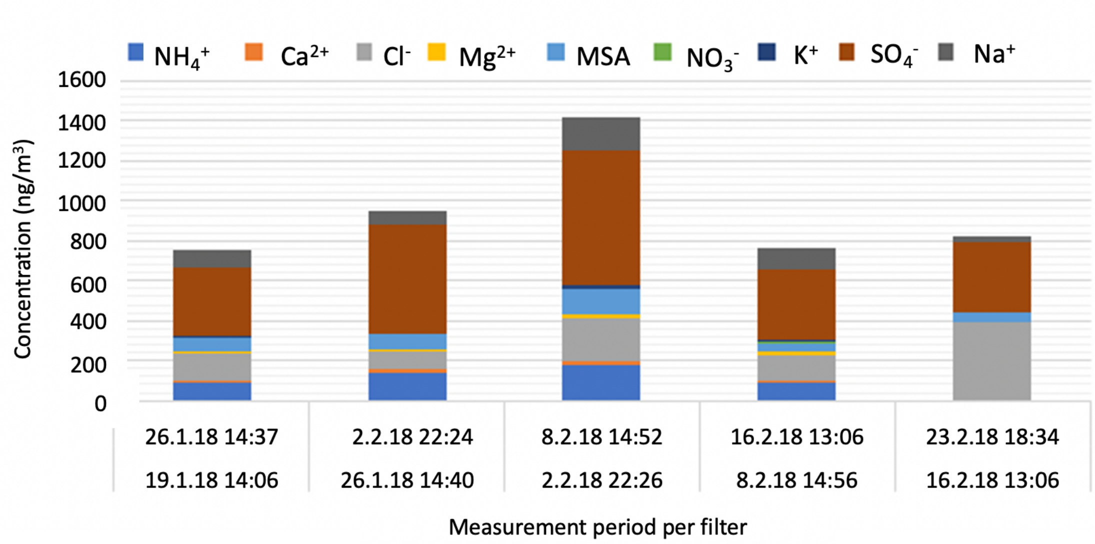

Figure 8: Chemical composition of water-soluble ions from weekly fine aerosol samples ($PM_{2.5}$)

Asmi et al. (2018) reported aerosol chemical composition from weekly filter analysis containing marine–originated sea salt aerosols and the presence of ammonium, sulfate, nitrate and mesylate ($CH_3SO_3^-$). Here, we performed the identical analysis, which agrees with the previously reported results.

Until February 16th, the fine aerosol composition remains rather constant with high amounts of non-sea salt sulphate (nss-sulphate, i.e., sulphate - 0.246 × sodium - in mass concentration, Brewer (1975)) which is partly neutralized by ammonia and a significant contribution from secondary marine MSA. The presence of Na^+, Cl^- and Ca^{2+} ions also indicates contribution from primary marine sea salt and continental soil minerals. Aerosol composition and mass concentrations are very similar to those found in Asmi et al. (2018) for Marambio summer aerosol. The highest concentrations of ions are measured during the active nucleation period in the beginning of February. By the end of the month, the concentrations of MSA, ammonium and calcium ions decrease. No indication of anthropogenic contamination is found in the samples.

The bulk aerosol chemical composition (Fig. 8) reflects rather well the observed cycle of the secondary particle formation and provides further evidence of the important role of sulphate/SA, methane sulfonate, and ammonia in the production and especially in the growth of Antarctic secondary aerosol. The qualitative agreement of gas-phase and particle-phase compositions indicates that it is likely possible that these compounds originate from similar marine/coastal sources.

3.3.4 Source of gas-phase precursors

Backward trajectories from sampled air masses (Fig. 9) were analyzed and seen to originate mostly from the West sector passing through the Southern Ocean before surrounding the Peninsula from its Northwest side - coinciding with the observed wind directions. The observed trajectories could explain the low concentration of IA, whose variability was independent of NPF occurrence due to (1) the absence of travel over the Weddell littoral seaside prior to the NPF or (2) because the algae bloom on the melting sea ice – possibly responsible for an increase reactive iodine of organic origin- has already occurred earlier in the season. On the other hand, the air is clearly enriched in MSA and SA when passing over the ocean that has the highest DMS concentration over the Dec-Feb months (Lana et al., 2011). In some instances, air mass trajectories are seen to turn over the North of the peninsula, which can indicate a possible enrichment of gas produced by the fauna on the land or at the shore (e.g., local source of ammonia and amines from penguin colony established at approx. 8 km South of the sampling site during summertime). With a majority of trajectories originating from the Bellingshausen Sea, NH_3 and various type of amines likely originate from the (melting) ocean as discussed in Dall'Osto et al. (2017).

Figure 9c also shows altitudes of the air mass trajectories. While (Kerminen et al., 2018) reviewed that Antarctic NPF would easily take place within the free troposphere, both the number size distribution and the indicated altitude flight path point toward nucleation processes occurring at the surface layer considering the lifetime (λ) of key gas-phase precursors (e.g., $\lambda_{SA} < 0.5$ h, Fiedler et al. (2005)). Similar back trajectories were calculated for non-event days, separately for days with high SA concentrations (i.e., [SA] > 2×10^6 molecules cm^{-3}) and for days with lower SA (Fig. S5a-c and Fig. 5a'-c', respectively). The result of the analysis as well as the model characteristics are shown in the *Supplementary Information*.

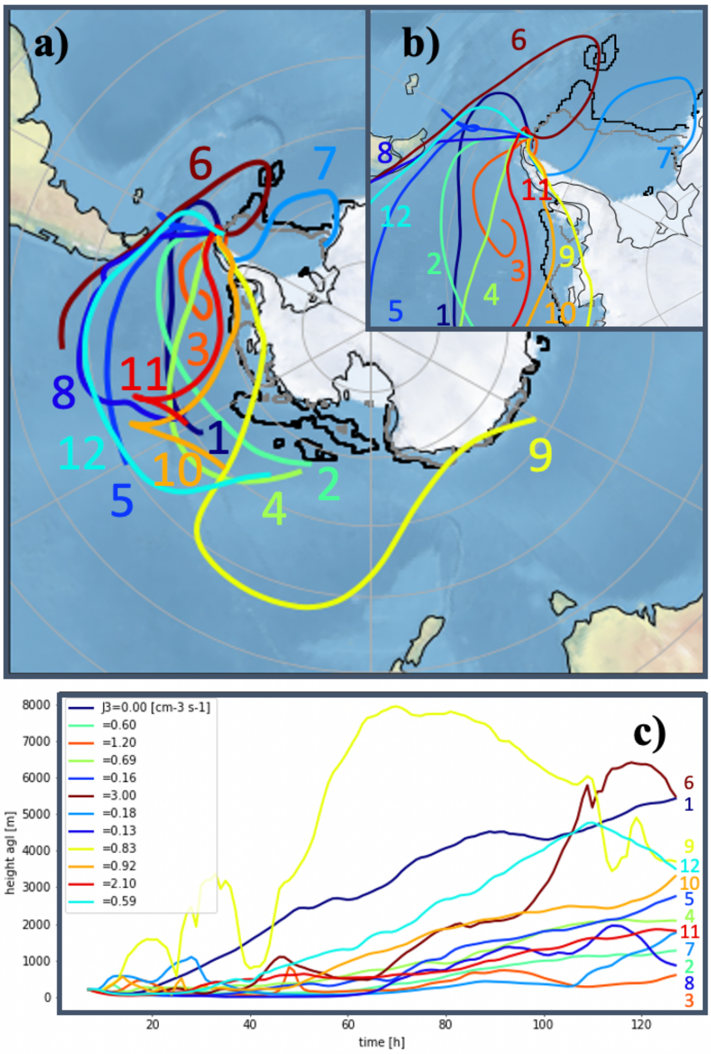

Figure 9: Backward trajectories for recorder NPF events a) (numbering according to classification Table 1). b) shows a zoom-in over the Antarctic Peninsula and c) shows the trajectory altitudes colored by formation rates J_3 values. In panel a) and b) the black and grey lines delimit the sea ice extent as average for January and February 2018, respectively. Sea ice data are from: ftp://sidads.colorado.edu/DATASETS/NOAA/G02135/south/monthly/ (Fetterer et al., 2017).

Local wind analysis (Fig. S6) was performed to determine possible local emission sources. In essence, no prevalent wind direction was found specifically for NPF days. However, in some instances, moderate to strong winds were seen to originate from the South/South-West sector where strong emission from the fauna is likely to occur by the shore at this season. Those days, 25 January (event # 3), 10 February (event # 9), and 11 Feb (event # 10), were among the highest growth ($GR_{3.8\text{-}12}$ = 10 nm h^{-1}) and the highest formation rates ($J_{1.5}$ = 10 cm^{-3} s^{-1} and $J_{1.5}$ = 9.2 cm^{-3} s^{-1}), respectively, which agree with our hypothesis attributing high emissions of e.g., ammonia / amines to the bird colony. On the other hand, Event #12 has a different trajectory and prevalent wind direction against the South sector. Given the fact that the anion mass defect (Fig.7) suggests significant presence of ammonia and possibly DMA on this event, specifically, nitrogen-containing base compounds origin can also be explained by bio-mechanism from the zoo/phytoplankton in the Antarctic Ocean.

4 Discussion

We observed the presence of many chemical constituents with significant measurable concentrations especially during aerosol formation events:

(1) IA daily maximum concentrations showed low variability, independent of NPF occurrence. Its concentration - only rarely over 10^6 molecules cm^{-3}- was unlikely sufficient to initiate NPF alone as compared with previously reported concentrations of 10^8 molecules cm^{-3} and (>) 8 × 10^6 molecules cm^{-3} for Arctic and coastal studies (Sipilä et al., 2016; Baccarini et al., 2020; Beck et al., 2021). Iodine emissions have been connected to sea-ice conditions and photolabile iodine compounds that are rapidly oxidized (Saiz-Lopez et al., 2015; He et al., 2021). The colder Weddell Sea provides high potential for the emission of iodine and thus iodic acid in the atmosphere. However, the temporality is a key factor governing such emissions. In fact, many studies have shown that IA concentration in polar-marine environment are usually peaking in early spring - already before the sea ice melt onset - (Saiz-Lopez et al., 2007) and during the refreezing transition period (Baccarini et al., 2020), strongly linking IA emissions with the sea ice state. This alternatively implies that our measurement period was then not optimum to catch iodine-related vapors maxima since the neighboring sea ice – key surface emission medium - was already melted around the Seymour Island. We do not exclude the possibility that IA would contribute to NPF in other seasons, but our data set show that during the austral summer period, from mid-January until the end of February, IA is likely not substantial.

The high concentrations of SA suggest that SA plays a key role in nucleation similarly to earlier observations from Antarctica (Jokinen et al., 2018) and from the Arctic (Beck et al., 2021). The significantly higher nucleation rates, with similar concentrations of SA, contrast with those studies that concluded that SA – ammonia ion induced nucleation was the primary pathway to new particle formation. The reported new particle formation rates were systematically below 1 cm^{-3} s^{-1}, typically ca. 2 orders of magnitude lower than observed in our study despite comparable air temperatures.

Taking the case study of 16 February as an example, we found sulfuric acid – ammonia complexes with high abundancy from the analysis of natural ion chemical composition (Fig. 7). That would indicate that at least negative ion-induced nucleation pathway proceeds with sequential addition of SA and NH_3. However, the total nucleation rate was 3.6 cm^{-3} s^{-1} on this day, much larger than the negative ion induced nucleation rate of 0.06 cm^{-3} s^{-1}. This would lead to the conclusion that a neutral nucleation mechanism could dominate the process in our case.

Outside the case study, nucleation rates are still remarkably high, often exceeding the ion-induced nucleation rate limit set by ion-production rate of ca. 2 ion pairs cm^{-3} s^{-1} by galactic cosmic radiation. While the exact nature of neutral mechanism is not directly detected, the parameterization experiments performed in the CERN CLOUD-chamber (Dunne et al., 2016; Kürten, 2019) indicate that very high concentrations of ammonia would be needed to explain the observed nucleation rates – above ppb levels, under assumption that the ternary SA-NH_3-H_2O mechanism was solely responsible for initial nucleation.

(2) Another possibility is that dimethyl amine – as detected in negative ion spectra (cf. Fig. 7) - efficiently nucleates with sulfuric acid and could be primarily responsible for neutral new particle SA-H_2O-DMA formation pathway, as discussed in several studies (Kürten et al., 2014; Brean et al., 2021). Unfortunately, the deployed instrumentation does not allow the determination of DMA concentrations to assess the exact contribution of DMA on nucleation. Yet, our observation shows significantly higher nucleation rates than the reported values of both studies and, considering the range of measured SA concentrations, this conjecture is not likely to happen alone but rather as a possible synergetic effect of both amines and ammonia in the nucleation with sulfuric acid and water at the encountered temperatures.

(3) In addition to the high quantity of SA and MSA measured in CI mode, MSA was observed in ion cluster in form of $CH_3SO_3^-$ and MSA clusters with bisulfate ion but not in any larger nucleating cluster. Its contribution to a possible ion-induced nucleation mechanism is therefore unlikely in our case. However, we still cannot exclude the possibility that MSA would be weakly bounded to ion clusters and then evaporated inside the mass spectrometer vacuum chambers and lost in semi-energetic collisions within the electric fields used to focus ions inside the system. Additionally, mesylate (i.e., the MSA fragments - $CH_3SO_3^-$) were observed in significant fraction in the chemical speciation of the aerosol phase, which indicates its involvement in particle growth.

(4) The missing link is the (high) concentration of ammonia and amines required to follow the proposed SA-(NH_3/DMA)-H_2O nucleation scheme, likely on the order of ppb for ammonia and ppt levels for DMA. Without direct measurement of neither NH_3 nor DMA, we can only speculate that our observations point toward a strong source, possibly land-based (e.g., from high penguin population during summertime) or marine-based (e.g., emissions from plankton's biological activity in the (melting) ocean). In fact, predominant wind possibly passing over a penguin colony at shore was seen from the wind roses proposed in Figure S6 for event 3, 4, 7, 9, and 10 and confirmed by the air mass trajectory analysis (Fig. 9). Yet, for our case study (event #12) - proving significant contribution of ammonia / DMA to detected in ion clusters -, nor the wind analysis nor

the backward trajectory analysis point toward emission sourcing from the bird colony. We do not exclude the possibility of additional influence from the local fauna, further away from the island, however this nitrogen-containing species could also be marine-sourced, especially by emission from the metabolic activity of planktons and accumulation of precursors (e.g., proteins) in the melting sea ice (Dall'Osto et al., 2017). Ammonia and amine concentrations are key parameters that need to be assessed to fully understand the nucleation mechanism that our analysis suggests.

(5) MSA, together with DMA, NH_3 and SA, could potentially nucleate via a neutral, yet unidentified mechanism. However, this potential mechanism does not manifest itself in chemical composition of negative ion clusters, and potentially would only occur as neutral. It is also important to consider that our measurement relies on clusters that are stable enough to be analyzed in the very low-pressure chamber of the TOF, and thus might not be detectable with all species or molecular cluster possibly present in the real atmosphere. Further investigations of nucleation potential of MSA including the aforementioned compounds as mixture are required before MSA can be attributed to be responsible for our observed high nucleation rates that we observe at Marambio.

(6) To this remains the question of organics; our data set do not show substantial presence of HOM (as characterized in forest environments), and possible detected compounds entering in our estimation – yet unidentified chemically, and which can also represent instrumental chemical background – could be low-volatility organic compounds originating from marine environment that may contribute to the growth to some extent (Weller et al., 2015; Kecorius et al., 2019).

(7) A possible explanation for our observations of higher-than-expected nucleation and growth rates is that particle formation and growth could occur primarily at colder temperatures at higher altitudes, which would enhance both SA-NH_3 and SA-DMA nucleation. Nucleated particles would then be transported to lower altitudes resulting in apparently higher nucleation and growth rates. This in turn suggest more regional emission sources rather than local emissions of SA, NH_3 or DMA as our analysis points toward. However, further investigations on vertical mixing would have been needed to confirm vertical distribution of nucleation and growth rates.

5 Conclusion

The Austral summer campaign 2018 at the Marambio Antarctic research station revealed very active aerosol processes and a frequency of new particle formation events of ~ 40 %. Out of 35 days of active measurement, a total of 13 NPF events were identified and characterized. In Marambio, NPF was promoted by key meteorological factors: high radiation (clear sky conditions), low humidity conditions (incl. the absence of precipitation), and high temperature – close to zero or above. We retrieved formation and growth rates for neutral and charged particles measured within 1.5 nm up to 800 nm size range - combining nCNC, NAIS and DMPS instrumentation. As a reference, the formation rate of 3-nm (neutral) particles (J_3) during NPF was on average 0.6863 cm^{-3} s^{-1} and the growth rate ($GR_{4\text{ -12 nm}}$) was on average 4.2 $nm.h^{-1}$. Those values are particularly high in comparison with the literature, the comparison remains even more surprising considering the most active NPF day where $J_{1.5}$ reached 19 $cm^{-3}s^{-1}$ and $GR_{4\text{ -12 nm}}$ was 10.9 $nm.h^{-1}$. The chemical analysis of gas-phase aerosol precursors with CI-APi-TOF showed high concentrations of SA and MSA - on average 5.17×10^5 molecules cm^{-3} and 1.18×10^6 molecules cm^{-3}, respectively – but quite low concentration of IA (on average 2.06×10^5 molecules cm^{-3}). All chemical species reached their maxima during mid-day (e.g., with maximum concentration of 2.56×10^7, 2.32×10^7 molecules.cm^{-3}, respectively for SA and MSA during aerosol formation events). The ubiquitously high SA concentration (peaking at almost 10^7 molecules cm^{-3} during many events) and the high abundancy of SA-associated ion clusters makes no doubt on the involvement of SA on NPF. The speciation of negative ion spectra revealed clusters of dimethylamine – sulfuric acid – bisulfate-ions, as well as various clusters of sulfuric acid - ammonia- bisulfate-ion - consistent with previously reported studies. However, the systematically high formation / growth rates cannot be quantitatively explained by SA-(DMA/ NH_3)-H_2O NPF pathways without direct measurement of DMA and NH_3 gas phase concentrations. Additionally, consistently high concentrations of MSA during daytime suggests a possible role of MSA in the growth, along with SA and ammonia - as confirmed by the bulk aerosol chemical composition. Herein, the mechanism of forming secondary aerosol in the peninsula involves a combination of SA, DMA, NH_3 and MSA (and only relatively low contribution of IA, at least at this time of the year). Better understanding the synergetic effect of DMA/NH_3 at these temperatures and environments require more field measurements and simulated experiments, specifically including direct measurement of DMA and NH_3 concentrations.

Data Availability

The key data set for both aerosol characterization and gas-phase composition are publically available on the Zenodo data repository platform:

Quéléver; L. L. J.; Dada, L.; Asmi, E.; Lampilahti, J.; Chan, T.; Ferrara, J.; Copes, G.; Pérez-Fogwill, G.; Barreira, L.; Aurela, M.; Worsnop, D.; Jokinen, T.; Sipilä, M.; (2022). Investigation of New Particle Formation mechanisms and aerosol processes at the Marambio Station, Antarctic Peninsula [Data set]. Zenodo. https://doi.org/10.5281/zenodo.6560413

For further information please contact Lauriane L. J. Quéléver (lauriane.quelever@helsinki.fi).

Acknowledgments

This work was supported by the European Research Council under the following programs: ERC (GASPARCON – grant n° 714621 & COALA – grant n° 638703) and EMME-CARE (grant n° 856612). We acknowledge the support from the Academy of Finland (projects n° 296628 and n° 328290), the Center of Excellence program (project n° 307331, 334514, 3282290), and Finnish Academy ACFA (project n° 335845 and ACCC Flagship funding (337552). We thank the generous help from the Servicio Meteorológico Nacional - SMN, the Fuerza Aerea Argentina - FAA, and the FINNish Antarctic Research Program – FINNARP. We are thankful for the technical personnel of the Marambio base for their support in cooperation, logistics and measurements. We thank Toftools for providing mass spectrometry analysis tool package for MATLAB.

Author's Contribution

EA and **MS** supervised the project. **EA** initiated the measurement container deployment and is responsible for the large size aerosol and auxiliary measurements data from the measurement container. **LLJQ** co-organized the project, prepared, set up and performed the measurements, analyzed the data, and wrote the manuscript. **LLJQ** operated the instrumentation with the help of **EA, JEF** and **GEC. EA, MS** and **TJ** supervised the analysis and contributed to the scientific discussion in collaboration with **DW. LLJQ** analyzed the gas-phase measurements and produced most figures. **LD** processed, analyzed, and discussed the aerosol phase data, prepared by **TC, JL, GPF** and **EA**. **LB** and **MA** analyzed the chemical composition of bulk aerosols**. EA** performed the backward trajectory analysis and its relevant figures. All co-authors contributed to the scientific discussion, commenting and the revision of the manuscript.

Competing interests

The authors claim no competing interests.

Supplementary Information (*cf. Separate file*)

References

Almeida, J., Schobesberger, S., Kürten, A., Ortega, I. K., Kupiainen-Määttä, O., Praplan, A. P., Adamov, A., Amorim, A., Bianchi, F., Breitenlechner, M., David, A., Dommen, J., Donahue, N. M., Downard, A., Dunne, E., Duplissy, J., Ehrhart, S., Flagan, R. C., Franchin, A., Guida, R., Hakala, J., Hansel, A., Heinritzi, M., Henschel, H., Jokinen, T., Junninen, H., Kajos, M., Kangasluoma, J., Keskinen, H., Kupc, A., Kurtén, T., Kvashin, A. N., Laaksonen, A., Lehtipalo, K., Leiminger, M., Leppä, J., Loukonen, V., Makhmutov, V., Mathot, S., McGrath, M. J., Nieminen, T., Olenius, T., Onnela, A., Petäjä, T., Riccobono, F., Riipinen, I., Rissanen, M., Rondo, L., Ruuskanen, T., Santos, F. D., Sarnela, N., Schallhart, S., Schnitzhofer, R., Seinfeld, J. H., Simon, M., Sipilä, M., Stozhkov, Y., Stratmann, F., Tomé, A., Tröstl, J., Tsagkogeorgas, G., Vaattovaara, P., Viisanen, Y., Virtanen, A., Vrtala, A., Wagner, P. E., Weingartner, E., Wex, H., Williamson, C., Wimmer, D., Ye, P., Yli-Juuti, T., Carslaw, K. S., Kulmala, M., Curtius, J., Baltensperger, U., Worsnop, D. R., Vehkamäki, H., and Kirkby, J.: Molecular understanding of sulphuric acid–amine particle nucleation in the atmosphere, Nature, 502, 359-363, 10.1038/nature12663, 2013.

Atkinson, H. M., Huang, R. J., Chance, R., Roscoe, H. K., Hughes, C., Davison, B., Schönhardt, A., Mahajan, A. S., Saiz-Lopez, A., Hoffmann, T., and Liss, P. S.: Iodine emissions from the sea ice of the Weddell Sea, Atmos. Chem. Phys., 12, 11229-11244, 10.5194/acp-12-11229-2012, 2012.

Asmi, E., Frey, A., Virkkula, A., Ehn, M., Manninen, H. E., Timonen, H., Tolonen-Kivimäki, O., Aurela, M., Hillamo, R., and Kulmala, M.: Hygroscopicity and chemical composition of Antarctic sub-micrometre aerosol particles and observations of new particle formation, Atmos. Chem. Phys., 10, 4253-4271, 10.5194/acp-10-4253-2010, 2010.

Asmi, E., Neitola, K., Teinilä, K., Rodriguez, E., Virkkula, A., Backman, J., Bloss, M., Jokela, J., Lihavainen, H., de Leeuw, G., Paatero, J., Aaltonen, V., Mei, M., Gambarte, G., Copes, G., Albertini, M., Fogwill, G. P., Ferrara, J., Barlasina, M. E., and Sánchez, R.: Primary sources control the variability of aerosol optical properties in the Antarctic Peninsula, Tellus B: Chemical and Physical Meteorology, 70, 1-16, 10.1080/16000889.2017.1414571, 2018.

Baccarini, A., Karlsson, L., Dommen, J., Duplessis, P., Vüllers, J., Brooks, I. M., Saiz-Lopez, A., Salter, M., Tjernström, M., Baltensperger, U., Zieger, P., and Schmale, J.: Frequent new particle formation over the high Arctic pack ice by enhanced iodine emissions, Nature Communications, 11, 4924, 10.1038/s41467-020-18551-0, 2020.

Barnes, I., Hjorth, J., and Mihalopoulos, N.: Dimethyl Sulfide and Dimethyl Sulfoxide and Their Oxidation in the Atmosphere, Chemical Reviews, 106, 940-975, 10.1021/acs.accounts.cr020529+, 2006.

Beck, L. J., Sarnela, N., Junninen, H., Hoppe, C. J. M., Garmash, O., Bianchi, F., Riva, M., Rose, C., Peräkylä, O., Wimmer, D., Kausiala, O., Jokinen, T., Ahonen, L., Mikkilä, J., Hakala, J., He, X.-C., Kontkanen, J., Wolf, K. K. E., Cappelletti, D., Mazzola, M., Traversi, R., Petroselli, C., Viola, A. P., Vitale, V., Lange, R., Massling, A., Nøjgaard, J. K., Krejci, R., Karlsson, L., Zieger, P., Jang, S., Lee, K., Vakkari, V., Lampilahti, J., Thakur, R. C., Leino, K., Kangasluoma, J., Duplissy, E.-M., Siivola, E., Marbouti, M., Tham, Y. J., Saiz-Lopez, A., Petäjä, T., Ehn, M., Worsnop, D. R., Skov, H., Kulmala, M., Kerminen, V.-M., and Sipilä, M.: Differing Mechanisms of New Particle Formation at Two Arctic Sites, Geophysical Research Letters, 48, e2020GL091334, 10.1029/2020GL091334, 2021.

Bianchi, F., Kurtén, T., Riva, M., Mohr, C., Rissanen, M. P., Roldin, P., Berndt, T., Crounse, J. D., Wennberg, P. O., Mentel, T. F., Wildt, J., Junninen, H., Jokinen, T., Kulmala, M., Worsnop, D. R., Thornton, J. A., Donahue, N., Kjaergaard, H. G., and Ehn, M.: Highly Oxygenated Organic Molecules (HOM) from Gas-Phase Autoxidation Involving Peroxy Radicals: A Key Contributor to Atmospheric Aerosol, Chemical Reviews, 119, 3472-3509, 10.1021/acs.chemrev.8b00395, 2019.

Bianchi, F., Tröstl, J., Junninen, H., Frege, C., Henne, S., Hoyle, C. R., Molteni, U., Herrmann, E., Adamov, A., Bukowiecki, N., Chen, X., Duplissy, J., Gysel, M., Hutterli, M., Kangasluoma, J., Kontkanen, J., Kürten, A., Manninen, H. E., Münch, S., Peräkylä, O., Petäjä, T., Rondo, L., Williamson, C., Weingartner, E., Curtius, J., Worsnop, D. R., Kulmala, M., Dommen, J., and Baltensperger, U.: New particle formation in the free troposphere: A question of chemistry and timing, Science, 352, 1109-1112, 10.1126/science.aad5456, 2016.

Bork, N., Elm, J., Olenius, T., and Vehkamäki, H.: Methane sulfonic acid-enhanced formation of molecular clusters of sulfuric acid and dimethyl amine, Atmos. Chem. Phys., 14, 12023-12030, 10.5194/acp-14-12023-2014, 2014.

Brean, J., Dall'Osto, M., Simó, R., Shi, Z., Beddows, D. C. S., and Harrison, R. M.: Open ocean and coastal new particle formation from sulfuric acid and amines around the Antarctic Peninsula, Nature Geoscience, 14, 383-388, 10.1038/s41561-021-00751-y, 2021.

Brewer, G. P.: Minor elements in seawater, Chemical Oceanography, 1, 415-496, 1975.

Chan, T., Cai, R., Ahonen, L. R., Liu, Y., Zhou, Y., Vanhanen, J., Dada, L., Chao, Y., Liu, Y., Wang, L., Kulmala, M., and Kangasluoma, J.: Assessment of particle size magnifier inversion methods to obtain the particle size distribution from atmospheric measurements, Atmos. Meas. Tech., 13, 4885-4898, 10.5194/amt-13-4885-2020, 2020.

Collins, D. B., Burkart, J., Chang, R. Y. W., Lizotte, M., Boivin-Rioux, A., Blais, M., Mungall, E. L., Boyer, M., Irish, V. E., Massé, G., Kunkel, D., Tremblay, J. É., Papakyriakou, T., Bertram, A. K., Bozem, H., Gosselin, M., Levasseur, M., and Abbatt, J. P. D.: Frequent ultrafine particle formation and growth in Canadian Arctic marine and coastal environments, Atmos. Chem. Phys., 17, 13119-13138, 10.5194/acp-17-13119-2017, 2017.

Dada, L., Chellapermal, R., Buenrostro Mazon, S., Paasonen, P., Lampilahti, J., Manninen, H. E., Junninen, H., Petäjä, T., Kerminen, V. M., and Kulmala, M.: Refined classification and characterization of atmospheric new-particle formation events using air ions, Atmos. Chem. Phys., 18, 17883-17893, 10.5194/acp-18-17883-2018, 2018.

Dada, L., Paasonen, P., Nieminen, T., Buenrostro Mazon, S., Kontkanen, J., Peräkylä, O., Lehtipalo, K., Hussein, T., Petäjä, T., Kerminen, V. M., Bäck, J., and Kulmala, M.: Long-term analysis of clear-sky new particle formation events and nonevents in Hyytiälä, Atmos. Chem. Phys., 17, 6227-6241, 10.5194/acp-17-6227-2017, 2017.

Dada, L., Lehtipalo, K., Kontkanen, J., Nieminen, T., Baalbaki, R., Ahonen, L., Duplissy, J., Yan, C., Chu, B., Petäjä, T., Lehtinen, K., Kerminen, V.-M., Kulmala, M., and Kangasluoma, J.: Formation and growth of sub-3-nm aerosol particles in experimental chambers, Nature Protocols, 15, 1013-1040, 10.1038/s41596-019-0274-z, 2020.

Dal Maso, M., Kulmala, M., Riipinen, I., Wagner, R., Hussein, T., Aalto, P. P., and Lehtinen, K. E.: Formation and growth of fresh atmospheric aerosols: eight years of aerosol size distribution data from SMEAR II, Hyytiala, Finland, Boreal Environment Research, 10, 323, 2005.

Dall'Osto, M., Beddows, D. C. S., Tunved, P., Harrison, R. M., Lupi, A., Vitale, V., Becagli, S., Traversi, R., Park, K. T., Yoon, Y. J., Massling, A., Skov, H., Lange, R., Strom, J., and Krejci, R.: Simultaneous measurements of aerosol size distributions at three sites in the European high Arctic, Atmos. Chem. Phys., 19, 7377-7395, 10.5194/acp-19-7377-2019, 2019.

Dall´Osto, M., Geels, C., Beddows, D. C. S., Boertmann, D., Lange, R., Nøjgaard, J. K., Harrison, R. M., Simo, R., Skov, H., and Massling, A.: Regions of open water and melting sea ice drive new particle formation in North East Greenland, Scientific Reports, 8, 6109, 10.1038/s41598-018-24426-8, 2018.

Dall´Osto, M., Beddows, D. C. S., Tunved, P., Krejci, R., Ström, J., Hansson, H. C., Yoon, Y. J., Park, K.-T., Becagli, S., Udisti, R., Onasch, T., O´Dowd, C. D., Simó, R., and Harrison, R. M.: Arctic sea ice melt leads to atmospheric new particle formation, Scientific Reports, 7, 3318, 10.1038/s41598-017-03328-1, 2017.

Deng, C., Fu, Y., Dada, L., Yan, C., Cai, R., Yang, D., Zhou, Y., Yin, R., Lu, Y., Li, X., Qiao, X., Fan, X., Nie, W., Kontkanen, J., Kangasluoma, J., Chu, B., Ding, A., Kerminen, V.-M., Paasonen, P., Worsnop, D. R., Bianchi, F., Liu, Y., Zheng, J., Wang, L., Kulmala, M., and Jiang, J.: Seasonal Characteristics of New Particle Formation and Growth in Urban Beijing, Environmental Science & Technology, 54, 8547-8557, 10.1021/acs.est.0c00808, 2020.

Dunne, E. M., Gordon, H., Kürten, A., Almeida, J., Duplissy, J., Williamson, C., Ortega, I. K., Pringle, K. J., Adamov, A., Baltensperger, U., Barmet, P., Benduhn, F., Bianchi, F., Breitenlechner, M., Clarke, A., Curtius, J., Dommen, J., Donahue, N. M., Ehrhart, S., Flagan, R. C., Franchin, A., Guida, R., Hakala, J., Hansel, A., Heinritzi, M., Jokinen, T., Kangasluoma, J., Kirkby, J., Kulmala, M., Kupc, A., Lawler, M. J., Lehtipalo, K., Makhmutov, V., Mann, G., Mathot, S., Merikanto, J., Miettinen, P., Nenes, A., Onnela, A., Rap, A., Reddington, C. L., Riccobono, F., Richards, N. A., Rissanen, M. P., Rondo, L., Sarnela, N., Schobesberger, S., Sengupta, K., Simon, M., Sipilä, M., Smith, J. N., Stozkhov, Y., Tomé, A., Tröstl, J., Wagner, P. E., Wimmer, D., Winkler, P. M., Worsnop, D. R., and Carslaw, K. S.: Global atmospheric particle formation from CERN CLOUD measurements, Science, 354, 1119-1124, 10.1126/science.aaf2649, 2016.

Ehn, M., Thornton, J. A., Kleist, E., Sipilä, M., Junninen, H., Pullinen, I., Springer, M., Rubach, F., Tillmann, R., Lee, B., Lopez-Hilfiker, F., Andres, S., Acir, I.-H., Rissanen, M., Jokinen, T., Schobesberger, S., Kangasluoma, J., Kontkanen, J., Nieminen, T., Kurtén, T., Nielsen, L. B., Jørgensen, S., Kjaergaard, H. G., Canagaratna, M., Maso, M. D., Berndt, T., Petäjä, T., Wahner, A., Kerminen, V.-M., Kulmala, M., Worsnop, D. R., Wildt, J., and Mentel, T. F.: A large source of low-volatility secondary organic aerosol, Nature, 506, 476-479, 10.1038/nature13032, 2014.

Fetterer, F., K. Knowles, W. N. Meier, M. Savoie, and A. K. Windnagel. 2017, updated daily. *Sea Ice Index, Version 3*. [ftp://sidads.colorado.edu/DATASETS/NOAA/G02135/south/monthly/]. Boulder, Colorado USA. NSIDC: National Snow and Ice Data Center, 10.7265/N5K072F8, 2021 [last access: August 5, 2021].

Fiebig, M., Hirdman, D., Lunder, C. R., Ogren, J. A., Solberg, S., Stohl, A., and Thompson, R. L.: Annual cycle of Antarctic baseline aerosol: controlled by photooxidation-limited aerosol formation, Atmos. Chem. Phys., 14, 3083-3093, 10.5194/acp-14-3083-2014, 2014.

Fiedler, V., Dal Maso, M., Boy, M., Aufmhoff, H., Hoffmann, J., Schuck, T., Birmili, W., Hanke, M., Uecker, J., Arnold, F., and Kulmala, M.: The contribution of sulphuric acid to atmospheric particle formation and growth: a comparison between boundary layers in Northern and Central Europe, Atmos. Chem. Phys., 5, 1773-1785, 10.5194/acp-5-1773-2005, 2005.

He, X.-C., Tham, Y. J., Dada, L., Wang, M., Finkenzeller, H., Stolzenburg, D., Iyer, S., Simon, M., Kürten, A., Shen, J., Rörup, B., Rissanen, M., Schobesberger, S., Baalbaki, R., Wang, D. S., Koenig, T. K., Jokinen, T., Sarnela, N., Beck, L. J., Almeida, J., Amanatidis, S., Amorim, A., Ataei, F., Baccarini, A., Bertozzi, B., Bianchi, F., Brilke, S., Caudillo, L., Chen, D., Chiu, R., Chu, B., Dias, A., Ding, A., Dommen, J., Duplissy, J., El Haddad, I., Gonzalez Carracedo, L., Granzin, M., Hansel, A., Heinritzi, M., Hofbauer, V., Junninen, H., Kangasluoma, J., Kemppainen, D., Kim, C., Kong, W., Krechmer, J. E., Kvashin, A., Laitinen, T., Lamkaddam, H., Lee, C. P., Lehtipalo, K., Leiminger, M., Li, Z., Makhmutov, V., Manninen, H. E., Marie, G., Marten, R., Mathot, S., Mauldin, R. L., Mentler, B., Möhler, O., Müller, T., Nie, W., Onnela, A., Petäjä, T., Pfeifer, J., Philippov, M., Ranjithkumar, A., Saiz-Lopez, A., Salma, I., Scholz, W., Schuchmann, S., Schulze, B., Steiner, G., Stozhkov, Y., Tauber, C., Tomé, A., Thakur, R. C., Väisänen, O., Vazquez-Pufleau, M., Wagner, A. C., Wang, Y., Weber, S. K., Winkler, P. M., Wu, Y., Xiao, M., Yan, C., Ye, Q., Ylisirniö, A., Zauner-Wieczorek, M., Zha, Q., Zhou, P., Flagan, R. C., Curtius, J., Baltensperger, U., Kulmala, M., Kerminen, V.-M., Kurtén, T., Donahue, N. M., Volkamer, R., Kirkby, J., Worsnop, D. R., and Sipilä, M.: Role of iodine oxoacids in atmospheric aerosol nucleation, Science, 371, 589, 10.1126/science.abe0298, 2021.

Herenz, P., Wex, H., Mangold, A., Laffineur, Q., Gorodetskaya, I. V., Fleming, Z. L., Panagi, M., and Stratmann, F.: CCN measurements at the Princess Elisabeth Antarctica research station during three austral summers, Atmos. Chem. Phys., 19, 275-294, 10.5194/acp-19-275-2019, 2019.

Hodshire, A. L., Campuzano-Jost, P., Kodros, J. K., Croft, B., Nault, B. A., Schroder, J. C., Jimenez, J. L., and Pierce, J. R.: The potential role of methanesulfonic acid (MSA) in aerosol formation and growth and the associated radiative forcings, Atmos. Chem. Phys., 19, 3137-3160, 10.5194/acp-19-3137-2019, 2019.

IPCC, Stocker, T. F., Qin, D., Plattner, G.-K., Tignor, M., Allen, S. K., Boschung, J., Nauels, A., Xia, Y., Bex, V., and Midgley, P. M. (Eds.): Climate Change 2013: The Physical Science Basis. Contribution of Working Group I to the Fifth Assessment Report of the Intergovernmental Panel on Climate Change, Cambridge University Press, Cambridge, United Kingdom and New York, NY, USA, 1535 pp., 10.1017/CBO9781107415324, 2013.

Jokinen, T., Sipilä, M., Junninen, H., Ehn, M., Lönn, G., Hakala, J., Petäjä, T., Mauldin Iii, R. L., Kulmala, M., and Worsnop, D. R.: Atmospheric sulphuric acid and neutral cluster measurements using CI-APi-TOF, Atmos. Chem. Phys., 12, 4117-4125, 10.5194/acp-12-4117-2012, 2012.

Jokinen, T., Sipilä, M., Kontkanen, J., Vakkari, V., Tisler, P., Duplissy, E. M., Junninen, H., Kangasluoma, J., Manninen, H. E., Petäjä, T., Kulmala, M., Worsnop, D. R., Kirkby, J., Virkkula, A., and Kerminen, V. M.: Ion-induced sulfuric acid–ammonia nucleation drives particle formation in coastal Antarctica, Science Advances, 4, eaat9744, 10.1126/sciadv.aat9744, 2018.

Järvinen, E., Virkkula, A., Nieminen, T., Aalto, P. P., Asmi, E., Lanconelli, C., Busetto, M., Lupi, A., Schioppo, R., Vitale, V., Mazzola, M., Petäjä, T., Kerminen, V. M., and Kulmala, M.: Seasonal cycle and modal structure of particle number size distribution at Dome C, Antarctica, Atmos. Chem. Phys., 13, 7473-7487, 10.5194/acp-13-7473-2013, 2013.

Kangasluoma, J., Franchin, A., Duplissy, J., Ahonen, L., Korhonen, F., Attoui, M., Mikkilä, J., Lehtipalo, K., Vanhanen, J., Kulmala, M., and Petäjä, T.: Operation of the Airmodus A11 nano Condensation Nucleus Counter at various inlet pressures and various operation temperatures, and design of a new inlet system, Atmos. Meas. Tech., 9, 2977-2988, 10.5194/amt-9-2977-2016, 2016.

Kecorius, S., Vogl, T., Paasonen, P., Lampilahti, J., Rothenberg, D., Wex, H., Zeppenfeld, S., van Pinxteren, M., Hartmann, M., Henning, S., Gong, X., Welti, A., Kulmala, M., Stratmann, F., Herrmann, H., and Wiedensohler, A.: New particle formation and its effect on cloud condensation nuclei abundance in the summer Arctic: a case study in the Fram Strait and Barents Sea, Atmos. Chem. Phys., 19, 14339-14364, 10.5194/acp-19-14339-2019, 2019.

Kerminen, V.-M., Chen, X., Vakkari, V., Petäjä, T., Kulmala, M., and Bianchi, F.: Atmospheric new particle formation and growth: review of field observations, Environmental Research Letters, 13, 103003, 10.1088/1748-9326/aadf3c, 2018.

Kirkby, J., Curtius, J., Almeida, J., Dunne, E., Duplissy, J., Ehrhart, S., Franchin, A., Gagné, S., Ickes, L., Kürten, A., Kupc, A., Metzger, A., Riccobono, F., Rondo, L., Schobesberger, S., Tsagkogeorgas, G., Wimmer, D., Amorim, A., Bianchi, F., Breitenlechner, M., David, A., Dommen, J., Downard, A., Ehn, M., Flagan, R. C., Haider, S., Hansel, A., Hauser, D., Jud, W., Junninen, H., Kreissl, F., Kvashin, A., Laaksonen, A., Lehtipalo, K., Lima, J., Lovejoy, E. R., Makhmutov, V., Mathot, S., Mikkilä, J., Minginette, P., Mogo, S., Nieminen, T., Onnela, A., Pereira, P., Petäjä, T., Schnitzhofer, R., Seinfeld, J. H., Sipilä, M., Stozhkov, Y., Stratmann, F., Tomé, A., Vanhanen, J., Viisanen, Y., Vrtala, A., Wagner, P. E., Walther, H., Weingartner, E., Wex, H., Winkler, P. M., Carslaw, K. S., Worsnop, D. R., Baltensperger, U., and Kulmala, M.: Role of sulphuric acid, ammonia and galactic cosmic rays in atmospheric aerosol nucleation, Nature, 476, 429-433, 10.1038/nature10343, 2011.

Kirkby, J., Duplissy, J., Sengupta, K., Frege, C., Gordon, H., Williamson, C., Heinritzi, M., Simon, M., Yan, C., Almeida, J., Tröstl, J., Nieminen, T., Ortega, I. K., Wagner, R., Adamov, A., Amorim, A., Bernhammer, A.-K., Bianchi, F., Breitenlechner, M., Brilke, S., Chen, X., Craven, J., Dias, A., Ehrhart, S., Flagan, R. C., Franchin, A., Fuchs, C., Guida, R., Hakala, J., Hoyle, C. R., Jokinen, T., Junninen, H., Kangasluoma, J., Kim, J., Krapf, M., Kürten, A., Laaksonen, A., Lehtipalo, K., Makhmutov, V., Mathot, S., Molteni, U., Onnela, A., Peräkylä, O., Piel, F., Petäjä, T., Praplan, A. P., Pringle, K., Rap, A., Richards, N. A. D., Riipinen, I., Rissanen, M. P., Rondo, L., Sarnela, N., Schobesberger, S., Scott, C. E., Seinfeld, J. H., Sipilä, M., Steiner, G., Stozhkov, Y., Stratmann, F., Tomé, A., Virtanen, A., Vogel, A. L., Wagner, A. C., Wagner, P. E., Weingartner, E., Wimmer, D., Winkler, P. M., Ye, P., Zhang, X., Hansel, A., Dommen, J., Donahue, N. M., Worsnop, D. R., Baltensperger, U., Kulmala, M., Carslaw, K. S., and Curtius, J.: Ion-induced nucleation of pure biogenic particles, Nature, 533, 521-526, 10.1038/nature17953, 2016.

Kontkanen, J., Järvinen, E., Manninen, H. E., Lehtipalo, K., Kangasluoma, J., Decesari, S., Gobbi, G. P., Laaksonen, A., Petäjä, T., and Kulmala, M.: High concentrations of sub-3nm clusters and frequent new particle formation observed in the Po Valley, Italy, during the PEGASOS 2012 campaign, Atmos. Chem. Phys., 16, 1919-1935, 10.5194/acp-16-1919-2016, 2016.

Kulmala, M., Kontkanen, J., Junninen, H., Lehtipalo, K., Manninen, H. E., Nieminen, T., Petäjä, T., Sipilä, M., Schobesberger, S., and Rantala, P.: Direct observations of atmospheric aerosol nucleation, Science, 339, 943-946, 10.1126/science.1227385, 2013.

Kulmala, M., Petäjä, T., Nieminen, T., Sipilä, M., Manninen, H. E., Lehtipalo, K., Dal Maso, M., Aalto, P. P., Junninen, H., Paasonen, P., Riipinen, I., Lehtinen, K. E. J., Laaksonen, A., and Kerminen, V.-M.: Measurement of the nucleation of atmospheric aerosol particles, Nature Protocols, 7, 1651-1667, 10.1038/nprot.2012.091, 2012.

Kulmala, M., Stolzenburg, D., Dada, L., Cai, R., Kontkanen, J., Yan, C., Kangasluoma, J., Ahonen, L. R., Gonzalez-Carracedo, L., Sulo, J., Tuovinen, S., Deng, C., Li, Y., Lehtipalo, K., Lehtinen, K. E. J., Petäjä, T., Winkler, P. M., Jiang, J., and Kerminen, V.-M.: Towards a concentration closure of sub-6 nm aerosol particles and sub-3 nm atmospheric clusters, Journal of Aerosol Science, 159, 105878, 10.1016/j.jaerosci.2021.105878, 2022.

Kyrö, E. M., Kerminen, V. M., Virkkula, A., Dal Maso, M., Parshintsev, J., Ruíz-Jimenez, J., Forsström, L., Manninen, H. E., Riekkola, M. L., Heinonen, P., and Kulmala, M.: Antarctic new particle formation from continental biogenic precursors, Atmos. Chem. Phys., 13, 3527-3546, 10.5194/acp-13-3527-2013, 2013.

Kürten, A.: New particle formation from sulfuric acid and ammonia: nucleation and growth model based on thermodynamics derived from CLOUD measurements for a wide range of conditions, Atmos. Chem. Phys., 19, 5033-5050, 10.5194/acp-19-5033-2019, 2019.

Kürten, A., Jokinen, T., Simon, M., Sipilä, M., Sarnela, N., Junninen, H., Adamov, A., Almeida, J., Amorim, A., Bianchi, F., Breitenlechner, M., Dommen, J., Donahue, N. M., Duplissy, J., Ehrhart, S., Flagan, R. C., Franchin, A., Hakala, J., Hansel, A., Heinritzi, M., Hutterli, M., Kangasluoma, J., Kirkby, J., Laaksonen, A., Lehtipalo, K., Leiminger, M., Makhmutov, V., Mathot, S., Onnela, A., Petäjä, T., Praplan, A. P., Riccobono, F., Rissanen, M. P., Rondo, L., Schobesberger, S., Seinfeld, J. H., Steiner, G., Tomé, A., Tröstl, J., Winkler, P. M., Williamson, C., Wimmer, D., Ye, P., Baltensperger, U., Carslaw, K. S., Kulmala, M., Worsnop, D. R., and Curtius, J.: Neutral molecular cluster formation of sulfuric acid–dimethylamine observed in real time under atmospheric conditions, Proceedings of the National Academy of Sciences, 111, 15019, 10.1073/pnas.1404853111, 2014.

Lachlan-Cope, T., Beddows, D. C. S., Brough, N., Jones, A. E., Harrison, R. M., Lupi, A., Yoon, Y. J., Virkkula, A., and Dall'Osto, M.: On the annual variability of Antarctic aerosol size distributions at Halley Research Station, Atmos. Chem. Phys., 20, 4461-4476, 10.5194/acp-20-4461-2020, 2020.

Lana, A., Bell, T. G., Simó, R., Vallina, S. M., Ballabrera-Poy, J., Kettle, A. J., Dachs, J., Bopp, L., Saltzman, E. S., Stefels, J., Johnson, J. E., and Liss, P. S.: An updated climatology of surface dimethlysulfide concentrations and emission fluxes in the global ocean, Global Biogeochemical Cycles, 25, 10.1029/2010GB003850, 2011.

Lehtipalo, K., Leppa, J., Kontkanen, J., Kangasluoma, J., Franchin, A., Wimnner, D., Schobesberger, S., Junninen, H., Petaja, T., and Sipila, M.: Methods for determining particle size distribution and growth rates between 1 and 3 nm using the Particle Size Magnifier, Boreal Environment Research, 2014.

Lehtipalo, K., Ahonen, L. R., Baalbaki, R., Sulo, J., Chan, T., Laurila, T., Dada, L., Duplissy, J., Miettinen, E., Vanhanen, J., Kangasluoma, J., Kulmala, M., Petäjä, T., and Jokinen, T.: The standard operating procedure for Airmodus Particle Size Magnifier and nano-Condensation Nucleus Counter, Journal of Aerosol Science, 159, 105896, 10.1016/j.jaerosci.2021.105896, 2022.

Loo, B. W. and Cork, C. P.: Development of High Efficiency Virtual Impactors, Aerosol Science and Technology, 9, 167-176, 10.1080/02786828808959205, 1988.

Manninen, H. E., Mirme, S., Mirme, A., Petäjä, T., and Kulmala, M.: How to reliably detect molecular clusters and nucleation mode particles with Neutral cluster and Air Ion Spectrometer (NAIS), Atmos. Meas. Tech., 9, 3577-3605, 10.5194/amt-9-3577-2016, 2016.

Mardyukov, A. and Schreiner, P. R.: Atmospherically Relevant Radicals Derived from the Oxidation of Dimethyl Sulfide, Accounts of Chemical Research, 51, 475-483, 10.1021/acs.accounts.7b00536, 2018.

Merikanto, J., Spracklen, D. V., Mann, G. W., Pickering, S. J., and Carslaw, K. S.: Impact of nucleation on global CCN, Atmos. Chem. Phys., 9, 8601-8616, 10.5194/acp-9-8601-2009, 2009.

Mirme, S. and Mirme, A.: The mathematical principles and design of the NAIS – a spectrometer for the measurement of cluster ion and nanometer aerosol size distributions, Atmos. Meas. Tech., 6, 1061-1071, 10.5194/amt-6-1061-2013, 2013.

Notz, D.: The future of ice sheets and sea ice: Between reversible retreat and unstoppable loss, Proceedings of the National Academy of Sciences, 106, 20590-20595, 10.1073/pnas.0902356106, 2009.

Saiz-Lopez, A. and von Glasow, R.: Reactive halogen chemistry in the troposphere, Chemical Society Reviews, 41, 6448-6472, 10.1039/C2CS35208G, 2012.

Saiz-Lopez, A., Blaszczak-Boxe, C. S., and Carpenter, L. J.: A mechanism for biologically induced iodine emissions from sea ice, Atmos. Chem. Phys., 15, 9731-9746, 10.5194/acp-15-9731-2015, 2015.

Saiz-Lopez, A., Mahajan Anoop, S., Salmon Rhian, A., Bauguitte Stephane, J. B., Jones Anna, E., Roscoe Howard, K., and Plane John, M. C.: Boundary Layer Halogens in Coastal Antarctica, Science, 317, 348-351, 10.1126/science.1141408, 2007.

Schmale, J., Baccarini, A., Thurnherr, I., Henning, S., Efraim, A., Regayre, L., Bolas, C., Hartmann, M., Welti, A., Lehtipalo, K., Aemisegger, F., Tatzelt, C., Landwehr, S., Modini, R. L., Tummon, F., Johnson, J. S., Harris, N., Schnaiter, M., Toffoli, A., Derkani, M., Bukowiecki, N., Stratmann, F., Dommen, J., Baltensperger, U., Wernli, H., Rosenfeld, D., Gysel-Beer, M., and Carslaw, K. S.: Overview of the Antarctic Circumnavigation Expedition: Study of Preindustrial-like Aerosols and Their Climate Effects (ACE-SPACE), Bulletin of the American Meteorological Society, 100(11), 2260-2283, 10.1175/BAMS-D-18-0187.1, 2019.

Schobesberger, S., Junninen, H., Bianchi, F., Lönn, G., Ehn, M., Lehtipalo, K., Dommen, J., Ehrhart, S., Ortega, I., Franchin, A., Nieminen, T., Riccobono, F., Hutterli, M., Duplissy, J., Almeida, J., Amorim, A., Breitenlechner, M., Downard, A., Dunne, E., and Worsnop, D.: Molecular understanding of atmospheric particle formation from sulfuric acid and large oxidized organic molecules, Proceedings of the National Academy of Sciences of the United States of America, 10.1073/pnas.1306973110, 2013.

Schobesberger, S., Franchin, A., Bianchi, F., Rondo, L., Duplissy, J., Kürten, A., Ortega, I. K., Metzger, A., Schnitzhofer, R., Almeida, J., Amorim, A., Dommen, J., Dunne, E. M., Ehn, M., Gagné, S., Ickes, L., Junninen, H., Hansel, A., Kerminen, V. M., Kirkby, J., Kupc, A., Laaksonen, A., Lehtipalo, K., Mathot, S., Onnela, A., Petäjä, T., Riccobono, F., Santos, F. D., Sipilä, M., Tomé, A., Tsagkogeorgas, G., Viisanen, Y., Wagner, P. E., Wimmer, D., Curtius, J., Donahue, N. M., Baltensperger, U., Kulmala, M., and Worsnop, D. R.: On the composition of ammonia–sulfuric-acid ion clusters during aerosol particle formation, Atmos. Chem. Phys., 15, 55-78, 10.5194/acp-15-55-2015, 2015.

Shaw, G. E.: Considerations on the origin and properties of the Antarctic aerosol, Reviews of Geophysics, 17, 1983-1998, 10.1029/RG017i008p01983, 1979.

Shaw, G. E.: Antarctic aerosols: A review, Reviews of Geophysics, 26, 89-112, 10.1029/RG026i001p00089, 1988.

Sipilä, M., Berndt, T., Petäjä, T., Brus, D., Vanhanen, J., Stratmann, F., Patokoski, J., Mauldin, R. L., Hyvärinen, A.-P., Lihavainen, H., and Kulmala, M.: The Role of Sulfuric Acid in Atmospheric Nucleation, Science, 327, 1243, 10.1126/science.1180315, 2010.

Sipilä, M., Sarnela, N., Neitola, K., Laitinen, T., Kemppainen, D., Beck, L., Duplissy, E. M., Kuittinen, S., Lehmusjärvi, T., Lampilahti, J., Kerminen, V. M., Lehtipalo, K., Aalto, P. P., Keronen, P., Siivola, E., Rantala, P. A., Worsnop, D. R., Kulmala, M., Jokinen, T., and Petäjä, T.: Wintertime sub-arctic new particle formation from Kola Peninsula sulphur emissions, Atmos. Chem. Phys. Discuss., 2021, 1-27, 10.5194/acp-2020-1202, 2021.

Sipilä, M., Sarnela, N., Jokinen, T., Henschel, H., Junninen, H., Kontkanen, J., Richters, S., Kangasluoma, J., Franchin, A., Peräkylä, O., Rissanen, M. P., Ehn, M., Vehkamäki, H., Kurten, T., Berndt, T., Petäjä, T., Worsnop, D., Ceburnis, D., Kerminen, V.-M., Kulmala, M., and O'Dowd, C.: Molecular-scale evidence of aerosol particle formation via sequential addition of HIO3, Nature, 537, 532-534, 10.1038/nature19314, 2016.

Stuecker, M. F., Bitz, C. M., Armour, K. C., Proistosescu, C., Kang, S. M., Xie, S.-P., Kim, D., McGregor, S., Zhang, W., Zhao, S., Cai, W., Dong, Y., and Jin, F.-F.: Polar amplification dominated by local forcing and feedbacks, Nature Climate Change, 8, 1076-1081, 10.1038/s41558-018-0339-y, 2018.

Vanhanen, J., Mikkilä, J., Lehtipalo, K., Sipilä, M., Manninen, H. E., Siivola, E., Petäjä, T., and Kulmala, M.: Particle Size Magnifier for Nano-CN Detection, Aerosol Science and Technology, 45, 533-542, 10.1080/02786826.2010.547889, 2011.

Virkkula, A., Asmi, E., Teinilä, K., Frey, A., Aurela, M., Timonen, H., Mäkelä, T., Samuli, A., Hillamo, R., Aalto, P., Kirkwood, S., and Kulmala, M.: Review of Aerosol Research at the Finnish Antarctic Research Station Aboa and its Surroundings in Queen Maud Land, Antarctica, Geophysica, 45, 2009.

Von Berg, L., Prend, C. J., Campbell, E. C., Mazloff, M. R., Talley, L. D., and Gille, S. T.: Weddell Sea Phytoplankton Blooms Modulated by Sea Ice Variability and Polynya Formation, Geophysical Research Letters, 47, e2020GL087954, 10.1029/2020GL087954, 2020.

Weller, R., Schmidt, K., Teinilä, K., and Hillamo, R.: Natural new particle formation at the coastal Antarctic site Neumayer, Atmos. Chem. Phys., 15, 11399-11410, 10.5194/acp-15-11399-2015, 2015.

Wiedensohler, A., Birmili, W., Nowak, A., Sonntag, A., Weinhold, K., Merkel, M., Wehner, B., Tuch, T., Pfeifer, S., Fiebig, M., Fjäraa, A. M., Asmi, E., Sellegri, K., Depuy, R., Venzac, H., Villani, P., Laj, P., Aalto, P., Ogren, J. A., Swietlicki, E., Williams, P., Roldin, P., Quincey, P., Hüglin, C., Fierz-Schmidhauser, R., Gysel, M., Weingartner, E., Riccobono, F., Santos, S., Grüning, C., Faloon, K., Beddows, D., Harrison, R., Monahan, C., Jennings, S. G., O'Dowd, C. D., Marinoni, A., Horn, H. G., Keck, L., Jiang, J., Scheckman, J., McMurry, P. H., Deng, Z., Zhao, C. S., Moerman, M., Henzing, B., de Leeuw, G., Löschau, G., and Bastian, S.: Mobility particle size spectrometers: harmonization of technical standards and data structure to facilitate high quality long-term observations of atmospheric particle number size distributions, Atmos. Meas. Tech., 5, 657-685, 10.5194/amt-5-657-2012, 2012.

Willis, M. D., Burkart, J., Thomas, J. L., Köllner, F., Schneider, J., Bozem, H., Hoor, P. M., Aliabadi, A. A., Schulz, H., Herber, A. B., Leaitch, W. R., and Abbatt, J. P. D.: Growth of nucleation mode particles in the summertime Arctic: a case study, Atmos. Chem. Phys., 16, 7663-7679, 10.5194/acp-16-7663-2016, 2016.

Yan, C., Dada, L., Rose, C., Jokinen, T., Nie, W., Schobesberger, S., Junninen, H., Lehtipalo, K., Sarnela, N., Makkonen, U., Garmash, O., Wang, Y., Zha, Q., Paasonen, P., Bianchi, F., Sipilä, M., Ehn, M., Petäjä, T., Kerminen, V. M., Worsnop, D. R., and Kulmala, M.: The role of H2SO4-NH3 anion clusters in ion-induced aerosol nucleation mechanisms in the boreal forest, Atmos. Chem. Phys., 18, 13231-13243, 10.5194/acp-18-13231-2018, 2018.

Yu, H., Ortega, J., Smith, J. N., Guenther, A. B., Kanawade, V. P., You, Y., Liu, Y., Hosman, K., Karl, T., Seco, R., Geron, C., Pallardy, S. G., Gu, L., Mikkilä, J., and Lee, S.-H.: New Particle Formation and Growth in an Isoprene-Dominated Ozark Forest: From Sub-5 nm to CCN-Active Sizes, Aerosol Science and Technology, 48, 1285-1298, 10.1080/02786826.2014.984801, 2014.